SunQM-6s11: In {N,n} QM Field Theory, the Residue nLL State Caused Positive Precession May Be the Origin of Mercury's Perihelion Precession, the Sunspot Drift, the Elliptic/Parabolic/Hyperbolic Orbits (Including the Gravitational Lensing), etc.

Yi Cao
e-mail: yicaojob@yahoo.com. ORCID: 0000-0002-4425-039X

Abstract

In developing the {N,n} QM field theory, from the pure quantum mechanics (QM), I deduced out a positive precession for the circular orbital motion (see in SunQM-4). In the current paper, I used this positive precession to explain 1) the Mercury's perihelion precession; 2) the fast-flow zonal band on Jupiter's atmospheric surface. Then, using a newly developed concept (i.e., the "face-opposite-face locked binary orbital motion" in φ-1D bi-direction with the anti-parallel spin will automatically transform to be a θ-1D orbital uni-directional motion, see in SunQM-6s10), I further developed this positive precession to be a positive/negative precession cycle (also called the "Y*l*m cycle"), and it is driven by the half-cycle of m > 0 and half-cycle of m < 0 in the nLL QM state of the |n,*l*,m>. Then, I used it to explain the elliptic orbit motion (an Y*l*m cycle with the acceleration/deceleration cycle), the sunspot drift (an Y*l*m cycle with a period of 22 years), the continental drift (an Y*l*m cycle with a period longer than 10^5 years), etc. The results of these analysis made me to further hypothesize that: the residue nLL QM state's positive/negative precession may even be the origin of all elliptic/parabolic/hyperbolic orbits (including the gravitational lensing that belongs to a hyperbolic motion). It may be possible to use QM's positive precession at different (and combined) high-frequency n' to fully explain Mercury's perihelion precession (without using classical physics and/or general relativity (GR)). This work revealed that in a circular/elliptical orbital motion, QM not only may (intrinsically) generate a positive precession, but also may (intrinsically) generate a positive/negative precession cycle (i.e., the Y*l*m cycle). This work may also suggest that the QM and the GR are the two "faces" of the same "master mechanics". Finally, because of its completeness and self-consistence, I do believe that the {N,n} QM is qualified to be put into the "Feynman Pool" as one of the many co-existing QM theories.

Introduction

In August 2016, I discovered that the Solar system can be described by a brand new {N,n//6} quantum mechanical structure [1]. Based on that result, (during the 10 years of the closed-door research), I further (independently) developed a {N,n} QM theory, and showed that not only the formation of Solar system [1] ~ [16], but also the formation of the whole universe [17] ~ [25], may can be described by the {N,n} QM. (Note: As an independent scientist, some of my research work may belong to a citizen-scientist-leveled work). As part of the {N,n} QM development, I (independently) designed and developed a brand new {N,n} QM field theory (for any point-centered field, like a mass field, a force field, an energy field, etc.) [23] ~ [24], [26] ~ [34]. The foundation of this theory includes: the four fundamental forces (Gravity, Electromagnetic, Strong, Weak, abbreviated as G-, EM-, S-, W-forces) have been re-classified into three pairs of force (E/RFe-force, G/RFg-force; S/RFs-force, see SunQM-6); all point-centered fields (including the mass field, the force field, and the energy field) can be represented by the Schrodinger equation/solution (in form of non-Born probability as well as in form of a 3D spherical wave packet, see SunQM-6s4); the non-Born probability description (that equals to the re-explanation of the Born probability density) as the collection of all elliptical orbital tracks (or, the Born probability density map's contour lines can be re-explained as the trajectory of a motion electron, see SunQM-6s2's Fig-2), the spherical 3D wave packet description (with

each shell's diameter equivalent to about one wavelength of the matter wave), the dis-entanglement of the outmost shell of the 3D wave packet (i.e., the "general decaying" process, see SunQM-6s1, -6s2, -6s3), the "|nL0> elliptical/parabolic/hyperbolic orbital transition model" (see SunQM-6s2, -6s3), the seamless transformation between a quantum process and a continues process through moving the r_1 inward (see SunQM-5s2), the trick that using the high-frequency n' quantum number to pin-point any small region in the {N,n} QM field (see SunQM-3s11, SunQM-6s1, etc.), a new type of 3-body motion as the "face-to-face plus face-opposite-face two-level orbital motion" (see SunQM-6s10), etc. So, the {N,n} QM is constituted with two parts: the Bohr-QM part (with {N,n//q} structure added), and the Schrodinger-equation-QM part (with RF, and {N,n} QM field theory added). Furthermore, by using {N,n} QM and the r'rθφ-4D space, I may be able to explain the possible origins of the lightspeed and its constancy (see SunQM-7s1 [35]), the $E = mc^2$, the length contraction in the special relativity, and the radial contraction in the general relativity, and even successfully fused the General Relativity's radial contraction calculation into the non-linear {N,n//q} QM structure's calculation at a black hole's surface (see SunQM-7s2 [36]). In SunQM-4, I found a (brand new) positive precession that can be generated through a pure QM process (in a nLL QM state circular orbital motion). In the current paper, I used this (pure QM generated) positive precession to explain the possible origins of the Mercury perihelion precession, the Jupiter surface's fast-flow zonal bands, the sunspot drift, the continental drift, the general elliptic/parabolic/hyperbolic orbits (even including the gravitational lensing), etc.

Note: **QM** means Quantum Mechanics, **RF** means "**R**ota**F**usion" (or rotation diffusion), **BH** means "black hole", **GR** means "general relativity", and **SR** means "Special relativity", |n*l*m> means |n,*l*,m> QM state, "**nLL**" or |nLL> means |n,*l*,m> QM state with *l* = n-1 = L, and *m* = n-1 = L. "**nL0**" or |nL0> means |n,*l*,m> QM state with *l* = n-1 = L, and m = 0. For {N,n} QM nomenclature as well as the general notes, please see SunQM-1's sections VII & VIII. Note: The best reading sequence for the (37 posted) SunQM series papers is: SunQM-1, 1s1, 1s2, 1s3, 2, 3, 3s1, 3s2, 3s6, 3s7, 3s8, 3s3, 3s9, 3s4, 3s10, 3s11, 4, 4s1, 4s2, 5, 5s1, 5s2, 7, 6, 6s1, 6s2, 6s3, 6s4, 6s5, 6s6, 6s7, 6s8, 6s10, 6s10, 6s11, 7s1, and 7s2. Note: for all SunQM series papers, reader should check "SunQM-9s1: Updates and Q/A for SunQM series papers" for the most recent updates and corrections. Note: Microsoft Excel's number format is often used in this paper, for example: x^2 = x^2, 3.4E+12 = $3.4*10^{12}$ = 3.4×10^{12}, 5.6E-9 = $5.6*10^{-9}$. Note: In previous SunQM papers, the current paper was often cited as "SunQM-4s4: More explanations on non-Born probability (NBP)'s positive precession in {N,n}QM. (in drafting since 2020)".

I. In {N,n} QM, the residue nLL state caused positive precession may be the origin of Mercury's perihelion precession

I-a. Review: A (full-QM deduced) non-Born probability (NBP) density at nLL state showed a positive precession

In the SunQM-3 series papers, I had demonstrated that our Solar system can be described by Schrodinger equation

$$i\hbar\frac{\partial}{\partial t}\Psi(r,\theta,\varphi,t) = \left[\frac{-\hbar^2}{2m}\nabla^2 + V(r,\theta,\varphi,t)\right]\Psi(r,\theta,\varphi,t) \qquad \text{eq-1 (SunQM-4's eq-1)}$$

In SunQM-4, after applied (what I called the "full-QM" deduction), and with

$$\Psi(r,\theta,\varphi,t) = R(r)T_r(t)\,\Theta(\theta)T_\theta(t)\,\Phi(\varphi)T_\varphi(t) = R(r)\Theta(\theta)\Phi(\varphi)T_\varphi(t) = R(r)Y(l,m)T_\varphi(t) \qquad \text{eq-2 (SunQM-4's eq-2)}$$

and

$$r^2\,|\Psi(r,\theta,\varphi,t)|^2 = r^2\,|R(r)|^2\,|\Theta(\theta)|^2\,|\Phi(\varphi)|^2\,|T_\varphi(t)|^2 \qquad \text{eq-3 (SunQM-4's eq-5)}$$

(where $T_r(t) = T_\theta(t) = 1$ was approximated for the planets that are doing the orbital motion in the Solar system, i.e., for the nLL QM state), I had deduced a time-dependent non-Born probability density for a planet in θφ-2D dimension of Solar system (for the nLL QM state only):

$$|Y(l,m,t)|^2 = |\Theta(\theta)|^2\,|\Phi(\varphi)|^2|T(t)|^2 \propto \left[\frac{1+\sin(\theta)}{2}\right]^{(n-1)} \left[\frac{1+\cos\left(\varphi - \frac{n}{n-1}\omega_n t\right)}{2}\right]^{n-1} \qquad \text{eq-4 (SunQM-4's eq-53)}$$

At n >> 1, n/(n-1) ≈ 1, eq-4 becomes

$$|Y(l,m,t)|^2 \propto \left[\frac{1+\sin(\theta)}{2}\right]^{n} \left[\frac{1+\cos(\varphi - \omega_n t)}{2}\right]^{n} \qquad \text{eq-5 (SunQM-4's eq-54)}$$

This means, when $n \to \infty$, the "Correspondence principle" of QM kicked-in, the QM result (in eq-4) does go back to the classical physics result, that is, for a circular orbital motion in φ-1D, its φ-1D position is φ - ωt. (Note: eq-4 and eq-5 are valid only for nLL QM state).

One of the most interesting results of this deduction is, after comparing to the classical physics in SunQM-3s11's eq-45 (in which a planet's φ-1D orbital position = φ - ωt), the QM formed eq-4 has the angular frequency/velocity

$$\frac{n}{n-1}\omega_n > \omega_n \qquad \text{eq-6}$$

at the nLL QM state (see SunQM-4's section I-h-3). Because in the nLL state, |m| = L = n - 1, eq-6 can also be re-written as

$$\frac{+|m|+1}{+|m|}\omega_n > \omega_n \qquad \text{eq-7}$$

Both eq-6 and eq-7 showed that, if this deduction of the time-dependent non-Born probability density is correct, then purely according to the quantum mechanics, there should be a positive precession for all (circular/elliptical) orbital moving planets. In other words, purely based on the QM, the positive precession is one of the intrinsic properties (or the natural attributes) of a circular/elliptic orbital motion. Then, **i**mmediately I thought that for the planet Mercury's perihelion precession (that in text books was always attributed to the classic physics effect plus the general relativity effect), maybe we can also explain it by using this pure QM effect of positive precession (as shown in the rest part of section I).

I-b. The nLL QM state, the (major) residue nLL QM state (that may produce the positive precession), and the minor nLL QM state (that may produce the positive/negative precession cycle)

Figure 1a showed the Born probability density radial distribution (at n = 1, 2, and 3) for a celestial body (that is plotted under the {N,n//q} QM structure within ΔN = 1, also see SunQM-6s6's Fig-1). We see that the n = 1 Born probability density (or the mass in |1,0,0> QM state) distributed mainly in between $r_{n=1}/r_1 = 1$ and $r_{n=2}/r_1 = 4$ (that means, between $r_{n=1}$ and $r_{n=2}$ shell, see the green solid curve in Figure 1a, or in the {N,1//q}o orbital shell); the n = 2 Born probability density (or the mass in |2,*l*,m> state) distributed mainly in between $r_{n=1}/r_1 = 4$ and $r_{n=2}/r_1 = 9$ (between $r_{n=2}$ and $r_{n=3}$ shell, see the red solid curve in Figure 1a, or in the {N,2//q}o orbital shell); the n = 3 Born probability density (or the mass in |3,*l*,m> state) distributed mainly in between $r_{n=2}/r_1 = 9$ and $r_{n=3}/r_1 = 16$ (between $r_{n=3}$ and $r_{n=4}$ shell, see the blue solid curve in Figure 1a, or in the {N,3//q}o orbital shell); and so on so forth. Based on it, (in SunQM-3s2) I proposed a simple rule to describe the relationship between the n and r_n (for the matter's QM state in a celestial body): "*all mass between r_n and r_{n+1} belongs to orbit n*".

However, for nLL QM state at n = 2, the mass in |2,1,1> QM state is mainly at around $r_{n=2}/r_1 = 4$ (see the red dashed curve in Figure 1a); for nLL QM state at n = 3, the mass in |3,2,2> QM state is mainly at around $r_{n=3}/r_1 = 9$ (see the blue dashed curve in Figure 1a), and so on so forth. Furthermore, for nLL at n = 2, we see that a significant part of |2,1,1> QM

state's mass located at $r/r_1 \leq 4$ (or at the outer edge of {0,1//q}o orbital shell, see the light-red shade Born probability density in Figure 1a). I named this part as the **residue nLL QM state**, or, the residue |2,1,1> QM state for n = 2, to emphasize that it is not located in n orbital shell, but at the outer edge of the n-1 orbital shell of the {N,n} structure. Similarly, for the residue nLL state at n = 3, that is, the residue |3,2,2> QM state's mass, it is distributed at $r/r_1 \leq 9$ (or at the outer edge of {0,2//q}o orbital shell, see the light-blue shade in Figure 1a), and so on so forth.

Then, in the {N,n} QM development for celestial bodies, I realized that the residue nLL QM state may correlate to a fast-flow stream that embedded on the surface equator of a {N,n//q} sized celestial ball (see in SunQM-6s4's Appendix A). For example, at the equator of the Sun surface, there is a stream rotating significantly faster (with a period of 25 days, see the white-colored region in Figure 1b) than the neighboring part (with a period of 27 days, see the red-colored region in Figure 1b) of the Sun. I believed that the mass in this fast-flow stream is in the residue |2,1,1> QM state, and it is the residue |2,1,1> QM state caused positive precession (see eq-4) that makes this stream to flow faster than the surroundings. Similarly, I believed that it is the residue |5,4,4> QM state caused positive precession (eq-4) that produced a fast-flow stream at the equator of the Jupiter surface (see Figure 2), and it is the residue |3,2,2> QM state caused positive precession (eq-4) that produced a fast-flow stream at the equator of the Saturn surface (see Figure 3). Therefore, based on eq-4, I hypothesized that all residue nLL QM states will have the positive precession that originated purely from the QM effect. In section-I and section-II, I used 8 examples to support this hypothesis.

Then, to explain the 22 years cycle of the sunspot drift (based on Babcock's magnetic dynamo model [37]), I further divided the residue nLL QM state into two parts: the major residue nLL QM state (that contains greater than 90% of the total residue nLL QM state, and with the constant positive precession), and the minor residue nLL QM state (that contains less than 10% of the total residue nLL QM state, and with a positive/negative precession cycle). Then, I hypothesized that the 22 years cycle of the sunspot drift is caused by the positive/negative precession cycle of the minor residue nLL QM state (i.e., the minor residue |2,1,1> QM state) of the Sun, while the major residue |2,1,1> keeps as a constant fast-flow at the equator of the Sun surface. In section-III, I used 4 examples to explain this hypothesis.

Note: In SunQM-3s9, the "primary zonal band" is now renamed as "the major residue nLL QM state", and the "secondary zonal band" is now rename as "the minor residue nLL QM state".

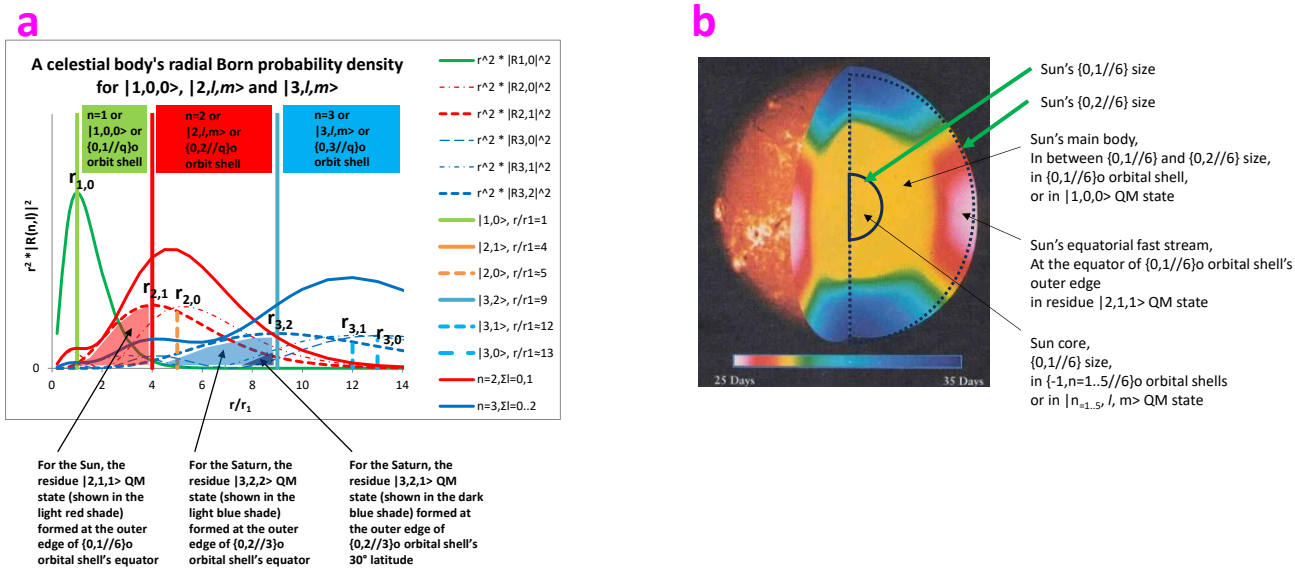

Figure 1a. The Born probability density radial distribution (at n = 1, 2, and 3) for a celestial body (that is plotted under the {N,n//q} QM structure within ΔN = 1).

Figure 1b. This cut-away picture of the Sun shows how the rate of solar rotation varies with depth and latitude. Copied from [38]. Authors (of the book): Neil F. Comins & William J. Kaufmann. Copy permission: granted by the author (of the book). The {N,n//6} QM structure was assigned by me.

I-c. Treat the observed perihelion precession of Mercury (and Venus, Earth, Mars) as the positive precession in the (major) residue nLL QM state

According to wiki "Mercury", "*The observed perihelion precession of Mercury is 5,600 arcseconds (1.5556°) per century relative to Earth, ... Newtonian mechanics, … predicts a precession of 5,557 arcseconds (1.5436°) per century relative to Earth, … Einstein's general theory of relativity provided … 42.980±0.001 arcseconds per century … for Mercury; ... Similar, but much smaller, effects exist for other Solar System bodies: 8.6247 arcseconds per century for Venus, 3.8387 for Earth, 1.351 for Mars*". (Note: As a citizen scientist, I don't know how to change Mercury precession value from "relative to Earth" to "relative to Solar system". Therefore, I simply assumed that "5600 arcseconds per century" is relative to the Solar system).

The orbit of {1,3//6} of the Mercury is either at the inner edge of {1,3//6}o orbital shell, or at the outer edge of {1,2//6}o orbital shell. Then, what it really belongs to, the {1,3//6}o orbit, or as the {1,2//6}o orbit? (Note: In SunQM-6s4's Appendix A-8, I asked the similar question for Earth's orbit). According to Figure 1a, Mercury was formed by accreting the mass mainly in the {1,3//6}o orbital shell, and minorly in the {1,2//6}o orbital shell. Then, we may can say that its orbit mainly belongs to the {1,3//6}o orbit, and can also be (minorly) treated as the residue nLL QM state of the {1,2//6}o orbital shell. So I hypothesized that the Mercury perihelion precession is caused by that Mercury's orbit can be (minorly) treated as the (major) residue |3,2,2> QM state of the {1,2//6}o orbital shell, and it is this (major) residue |3,2,2> QM state caused positive precession that really produced the positive precession of the Mercury perihelion. This hypothesis should also apply to all other planetary orbital motion's positive precessions.

I-d. Determine the quantum numbers of |m| and n' at the (major) residue nLL QM state (that caused positive precession) for Mercury (and Venus, Earth, Mars)'s perihelion procession

Example-1: Determine the (major) residue nLL QM state's |m| and n' value for Mercury's perihelion precession.

In {N,n//q} QM, planet Mercury is at {1,3//6} = {0,3*6//6} = {-1,3*6^2//6} = {2,(3/6)//6} QM state, or QM orbit, with the base-frequency n = 3, or high-frequency n' = 3*6 =18, or 3*6^2 =108, etc., or sub-base-frequency n' = 3/6, etc. Alternatively, we can use |n,*l*,m> at nLL QM state to describe Mercury's {1,3//6} orbit as |3,2,2>, or |18,17,17>, or |108,107,107>, etc., or, as the residue |3,2,2>, or residue |18,17,17>, or residue |108,107,107>, etc. Notice that in nLL state (and/or in residue nLL state), it is defined *l* = n-1 = L, |m| = n-1 = L. In this example, under the hypothesis that the perihelion precession of Mercury is caused by the positive precession of the (major) residue nLL QM, I want to determine the |m| quantum number (either |m|= n-1, or |m|= n'-1) for this (major) residue nLL QM state.

Mercury's orbital period is 88 days. It equals to (100 x 365.2 days / 88 days =) 415 rounds per 100 years. Each round's precession = 5600"/3600/415 = 0.00375°. While Mercury orbits one round = 360° (with the orbital speed $v_{orbit} \propto 1/360$), the orbital perihelion one round (with precession) = 360° + 0.00375° (with the orbital speed $v_{orbit+prec} \propto 1/(360 - 0.00375)$). (At a citizen scientist level), we can reasonably assume that the ratio of $\frac{n'}{n'-1} = \frac{+|m|+1}{+|m|}$ equals to the ratio of

$$\frac{n'}{n'-1} = \frac{+|m|+1}{+|m|} = \frac{v_{faster}}{v_{normal}} = \frac{1/T_{faster}}{1/T_{normal}} = \frac{T_{normal}}{T_{faster}} \qquad \text{eq-8}$$

where T is the period of the circular/elliptic orbital motion. Thus, eq-8 provides us a way to use the speed difference, between the (positive precession included) faster speed and the (positive precession un-included) normal speed, to determine the |m| and n' quantum number for the residue nLL QM state.

Then, from eq-8, we have $\frac{+|m|+1}{+|m|} = \frac{T_{normal}}{T_{faster}} = \frac{360}{(360-0.00375)}$, |m| ≈ 95999, n' = |m| + 1 ≈ 96000. At Mercury's orbit {1,3//6}, the residue nLL QM state should have either n = 3, or n' = 3*6^1= 18, or n' = 3*6^5 = 23328, or n' = 3*6^6 = 139968, etc. If I chose n' = 3*6^6 = 139968, then at the residue nLL = |3*6^6, 3*6^6-1, 3*6^6-1> state, or the residue

|139968,139967,139967> state, it will produce $\frac{n\prime}{n\prime-1}=\frac{139968}{139967}=\frac{360}{(360-x)}$, x = 0.002572° precession per round, or 3842 arcseconds per century. If I chose n' = 3*6^7 = 839808, then at the residue nLL = |839808, 839807, 839807> state, it will produce $\frac{n\prime}{n\prime-1}=\frac{839808}{839807}=\frac{360}{(360-x)}$, x = 0.0004287° precession per round, or 640.4 arcseconds per century. The results of n' = 3*6^5, 3*6^6, 3*6^7, 3*6^8, and 3*6^9 for Jupiter were listed in Table 1.

Table 1. Using eq-8 to determine the |m| and n' quantum numbers for the residue nLL QM state (that caused positive precession) for Mercury, Venus, Earth, and Mars's perihelion procession.

	Observed	Calculated			
planet orbital precession				$\frac{+\lvert m\rvert+1}{+\lvert m\rvert}=\frac{n'}{n'-1}=\frac{360}{(360-x)}$	
		pick n'=	m = n'-1	x=	
	"/100 yr			degree per round	"/100 yr
Mercury		3*6^5		0.015432099	23056
	5600	3*6^6		0.002572016	**3843**
		3*6^7		0.000428669	640.4
		3*6^8		0.000071445	106.7
		3*6^9		0.000011907	17.79
Venus		4*6^8		0.00005358	31.34
	8.6247	4*6^9		0.00000893	**5.22**
		4*6^10		0.00000149	0.87
Earth		5*6^8		0.00004287	15.43
	3.8387	5*6^9		0.00000715	**2.57**
		5*6^10		0.00000119	0.43
Mars		6*6^8		0.00003572	6.84
	1.351	6*6^9		0.00000595	**1.14**
		6*6^10		0.00000099	0.19

Example-2: Determine the (major) residue nLL QM state's |m| and n' value for Venus's perihelion precession.

Venus's orbital period is 224.7 days. It equals to (100 x 365.2 days / 224.7 days =) 162.6 rounds per 100 years. Each round's precession = 8.6247"/3600/162.6 = 0.00001474°. $\frac{+|m|+1}{+|m|}=\frac{T_{normal}}{T_{faster}}=\frac{360}{(360-0.00001474)}$, |m| ≈ 24422419. At Venus's orbit {1,4//6}, the residue nLL QM state should have either n = 4, or n' = 4*6^1= 24, or n' = 4*6^8 = 6718464, etc. If I chose n' = 4*6^8 = 6718464, then at the residue nLL = |4*6^8,4*6^8-1,4*6^8-1> state, it will produce $\frac{n\prime}{n\prime-1}=\frac{6718464}{6718463}=\frac{1/(360-x)}{1/360}$, x = 0.00005358° precession per round, or 31.34 arcseconds per century. The results of n' = 4*6^8, n' = 4*6^9, n' = 4*6^10 for Venus were listed in Table 1.

Example-3: Determine the (major) residue nLL QM state's |m| and n' value for Earth's perihelion precession.

Earth's orbital period 365.2 days. It equals to 100 x 365.2 days / 365.2 days = 100 rounds per 100 years. Each round precession = 3.8387"/3600/100 = 0.00001066°. $\frac{+|m|+1}{+|m|}=\frac{T_{normal}}{T_{faster}}=\frac{360}{(360-0.00001066)}$, |m| ≈ 33761429. At Earth's orbit {1,5//6} with base-n at 5, if I chose n' = 5*6^8 = 8398080, then at the residue nLL = |5*6^8, 5*6^8-1, 5*6^8-1> state, it will produce $\frac{n\prime}{n\prime-1}=\frac{8398080}{8398079}=\frac{1/(360-x)}{1/360}$, x = 0.00004287° precession per round, or 15.43 arcseconds per century. The results of n' = 5*6^8, n' = 5*6^9, n' = 5*6^10 for Earth were listed in Table 1.

Example-4: Determine the (major) residue nLL QM state's |m| and n' value for Mars's perihelion precession.

Mars's orbital period 687 days. It equals to (100 x 365.2 days / 687 days =) 53.16 rounds per 100 years. Each round precession = 1.351"/3600/53.16 = 0.00000706°. $\frac{+|m|+1}{+|m|}=\frac{T_{normal}}{T_{faster}}=\frac{360}{(360-0.00000706)}$, m ≈ 50994539. At Mars's orbit {1,6//6} with base-n at 6, if I chose n' = 6*6^8 = 10077696, then at the residue nLL = |6*6^8, 6*6^8-1, 6*6^8-1> state, it will produce

$\frac{n\prime}{n'-1} = \frac{10077696}{10077695} = \frac{1/(360-x)}{1/360}$, x = 0.00003572° precession per round, or 6.836 arcseconds per century. The results of n' = 6*6^8, n' = 6*6^9, n' = 6*6^10 for Mars were listed in Table 1.

If the calculations in Table 1 are correct, then can we attribute all the planetary elliptic orbital motion's positive precessions (in the Solar system) mainly as the pure quantum mechanics effect (i.e., the residue nLL QM state caused positive precession)? For example, we may can explain Mercury orbital motion's 5600"/100yr perihelion precession as:
1) Among 5600"/100yr, 3843"/100yr may come from the positive precession caused by the pure quantum mechanics effect at the residue nLL state (with high-frequency n'= 3*6^6, or with nLL QM state at $|n'_{=3*6\^6}, l_{=3*6\^6-1}, m_{=3*6\^6-1}>$, or within the high-frequency {6,3//6}o orbital shell), and the rest (5600-3843)"/100yr may come from other factors; Or, among 5600"/100yr, 640"/100yr may come from the residue nLL at $|n'_{=3*6\^7}, l_{=3*6\^7-1}, m_{=3*6\^7-1}>$ QM state's positive precession, or 106.7"/100yr may come from the residue nLL at $|n'_{=3*6\^8}, l_{=3*6\^8-1}, m_{=3*6\^8-1}>$ QM state's positive precession, or 17.79"/100yr may come from the residue nLL at $|n'_{=3*6\^9}, l_{=3*6\^9-1}, m_{=3*6\^9-1}>$ QM state's positive precession.
2) Furthermore, Table 1 suggested that we may can use the pure QM's positive precession at different (and combined) n' to fully explain Mercury's 5600"/100yr perihelion precession (without using classical physics and general relativity). E.g., at the perihelion region with a low n' = 3*6^5 state and the faster precession 23056"/100yr, and at the aphelion region with a high n' = 3*6^6 state and slower precession 3843"/100yr, and then averaged as the 5600"/100yr perihelion precession.
3) Similarly, for Venus's 8.6247"/100yr, Earth's 3.8387"/100yr, and Mars's 1.351"/100yr observed perihelion precession (see the green cells in Table 1), they may mainly come from Venus's residue nLL QM at $|n'_{=4*6\^9}, l_{=4*6\^9-1}, m_{=4*6\^9-1}>$ state's positive precession, the Earth's residue nLL QM at $|n'_{=5*6\^9}, l_{=5*6\^9-1}, m_{=5*6\^9-1}>$ state's positive precession, and the Mars's residue nLL QM at $|n'_{=6*6\^9}, l_{=6*6\^9-1}, m_{=6*6\^9-1}>$ state's positive precession, respectively (see the yellow cells in Table 1).

If the above explanations are correct, then the next big question is: what is the relationship between the nLL QM state's (or the residue nLL QM state's) positive precession, the Newtonian mechanics' positive precession, and the Einstein general relativity's positive precession? Are they actually the same thing but showed up in three theories as three different "faces" (just like that Heisenberg-initiated matrix mechanics and Schrodinger-initiated wave mechanics are actually the two "faces" of the same quantum mechanics)? I don't know the answer, although I hope so.

II. The same (major) residue nLL QM state caused positive precession may also be the origin of the fast-flow zonal bands on Jupiter (and Saturn, Earth, Sun) atmosphere surface

Example-5: For Jupiter surface's |5,4,4>, |5,4,3>, |5,4,2>, |5,4,1> fast-flow zonal bands, determine the residue nLL QM state's |m| and n' value.

As illustrated in Figure 2a and Figure 2b, the seven major zonal bands on the surface of Jupiter's atmosphere are in the |5,4,4> , |5,4,3>, |5,4,2>, |5,4,1> QM states, and they are embedded on the surface of Jupiter's atmosphere that is in the background |4,0,0> QM state (that appeared as the belt bands). According to SunQM-3s1's eq-1 ($\omega_{n-spin} = \frac{\omega_{1-spin}}{n^x}$), all Jupiter's zonal bands, because they are at n = 5 of the |5,4,m> QM state, they should have spin speed slower than that of the belt bands (in the |4,0,0> QM state with n=4). However, according to Figure 2c, all Jupiter's zonal bands have the observed (eastward spin) speed faster than that of the belt bands. In SunQM-6s4's Appendix-A, I named the "residue nLL QM state" for the |5,4,4> fast-flow zonal band that embedding on Jupiter's surface |4,0,0>. Broadly to say, all seven |5,4,m> fast-flow zonal bands that embedding on Jupiter's surface |4,0,0> can all be called as the "residue nLL QM state" in this case (although strictly to say, they should be called the "residue nLm QM state", with l = n-1 = L, and m = -l, … +l). Then, what makes these "residue nLL QM state" zonal bands to move at a speed faster than the normal background speed (on the surface of Jupiter atmosphere)? My hypothesis is: it is caused by the residue nLL QM state generated positive precession as shown in eq-4.

For Jupiter's |5,4,4> fast-flow zonal band at the equator, according to wiki "Atmosphere of Jupiter" (also shown in Figure 2c), it is ~130 m/s faster than Jupiter ball's equatorial (background) rotation velocity ~12600 m/s (see wiki "Jupiter"). Then, we can use eq-8, $\frac{+|m|+1}{+|m|} = \frac{v_{faster}}{v_{normal}} = \frac{12600+130}{12600}$, |m| ≈ 97 , n' = |m| + 1 ≈ 98. At Jupiter surface's equator, the residue |5,4,4> QM state should have either n = 5, or n' = 5*5^1 = 25, or n' = 5*5^2 = 125, etc. After an approximation, I chose n'= 5*5^2 = 125, m = n' - 1 ≈ 124, for the positive precession of the residue |5,4,4> QM state stream (but at high-frequency n' of |125,124,124> state), that will be $\frac{125}{124} = \frac{12600+x}{12600}$, x ≈ 102 m/s faster than the background 12600 m/s. It reasonably well matches the observed ~130 m/s speed.

For Jupiter's |5,4,3> fast-flow zonal band stream at θ' ≈ 20° latitude region, Jupiter ball's (background) rotation velocity at θ' ≈ 20° is cos(20°) * 12600 m/s ≈ 11840 m/s. From Figure 2c, |5,4,3> band was (read as) about 40 m/s faster than that of the background speed (11840 m/s). Assuming not only nLL = |5,4,4> QM state has the $\varphi = \frac{n'}{n'-1}\omega_n t = \frac{|m|+1}{|m|}\omega_n t$ positive precession effect (in eq-4), but |5,4,3> QM state also has the similar positive precession like $\varphi = \frac{n'}{n'-2}\omega_n t = \frac{+|m|+2}{+|m|}\omega_n t$, where n' = |m| + 2 for |n=5,*l*=4,m=3> . Also, assuming that $\frac{+|m|+2}{+|m|} = \frac{v_{|5,4,3>zonal\ band}}{v_{background}}$, then, we have $\frac{+|m|+2}{+|m|} = \frac{11840+40}{11840}$, |m| ≈ 592, n' = |m| + 2 ≈ 594. At Jupiter surface, the residue |5,4,3> QM state should have either n = 5, or n' = 5*5^1 = 25, or n' = 5*5^3 = 625, etc. After an approximation, I chose n'= 5*5^3 = 625 for the positive precession of the residue |5,4,3> QM state stream, that will be $\frac{625}{623} = \frac{11840+x}{11840}$, x ≈ 38.0 m/s faster than the background 11840 m/s. It well matches the observed ~40 m/s speed.

For Jupiter's |5,4,2> fast-flow zonal band stream at θ' ≈ 33° latitude region, Jupiter ball's rotation velocity at θ' ≈ 33° is cos(33°) * 12600 m/s ≈ 10567 m/s. From Figure 2c, |5,4,2> band was (read as) about 35 m/s faster than that of the background speed (10567 m/s). Using the similar method as that for |5,4,3> , we have $\frac{+|m|+3}{+|m|} = \frac{10567+35}{10567}$, |m| ≈ 906 , n' = |m| + 3 ≈ 909. At Jupiter surface, the residue |5,4,2> QM state should have either n = 5, or n' = 5*5^1 = 25, or n' = 5*5^3 = 625, etc. After an approximation, I chose n'= 5*5^3 = 625 for the positive precession of the residue |5,4,2> QM state stream, that will be $\frac{625}{622} = \frac{10567+x}{10567}$, x ≈ 51.0 m/s faster than the background 10567 m/s. It reasonably matches the observed ~35 m/s speed. All above results, plus the similar calculation for Jupiter's |5,4,1> fast-flow zonal band stream, were listed in Table 2.

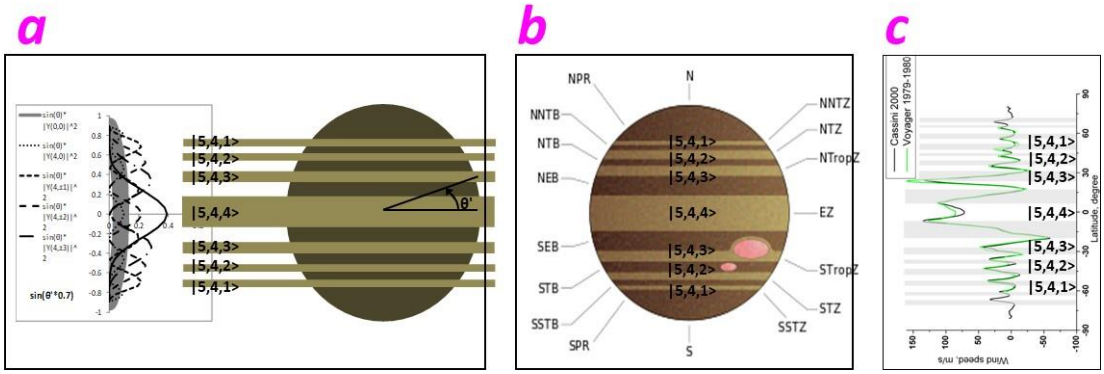

Figure 2a. For |5,4,m> QM states, to correlate the latitude positions between the calculated Born probability peaks and the observed Jupiter surface's zonal bands (see Figure 2b). Copied from SunQM-3s3's Fig-3b.
Figure 2b. Copied from wiki "Atmosphere of Jupiter" figure "Idealized illustration of Jupiter's cloud bands". Author: Sakurambo at English Wikipedia - Transferred from en.wikipedia to Commons by Shizhao using CommonsHelper. Copyright: Public Domain. Also shown in SunQM-3s3's Fig-3c, and analyzed as |5,4,m> by me.
Figure 2c. Copied from wiki "Atmosphere of Jupiter" figure "Zonal wind speeds in the atmosphere of Jupiter". Author: "Ruslik0". Copyright: CC BY-SA 3.0. Assigned as the |5,4,m> QM state by me.

Table 2. Determine the |m| and n' quantum number value, so that we can use the residue nLL QM state caused positive precession speed to match to the observed speed of the fast zonal band stream (on a planet's atmosphere surface).

	residue nLL QM state	n=	l=	m=	n-m=	latitude	backgroun d speed	observed fast speed	v_{fast} / v_{normal} =	|m|=	calculated |m| =	calculated n'= |m|+(n-m)=	chose n'=	chose n'=	residue nLL determined faster speed
						degree	m/s	m/s							m/s
Jupiter	|5,4,4>	5	4	4	1	0	12600	130	(|m|+1) / |m|	n'-1	96.92	98	5*5^2=	125	101.6
	|5,4,3>	5	4	3	2	20	11840.1	40	(|m|+2) / |m|	n'-2	592.01	594	5*5^3=	625	38.0
	|5,4,2>	5	4	2	3	33	10567.2	35	(|m|+3) / |m|	n'-3	905.76	909	5*5^3=	625	51.0
	|5,4,1>	5	4	1	4	42	9363.6	30	(|m|+4) / |m|	n'-4	1248.48	1252	5*5^3=	625	60.3
Saturn	|3,2,2>	3	2	2	1	0	9870	470	(|m|+1) / |m|	n'-1	21.00	22	3*3^2=	27	379.6
	|3,2,1>	3	2	1	2	30	8547.7	150	(|m|+2) / |m|	n'-2	113.97	116	3*3^3=	81	216.4
Earth,Polar jet	|3,2,1>	4	3	1	3	60	232.7	50	(|m|+3) / |m|	n'-3	13.96	17	3*3^1=	16	53.70
							T=days	days							days
Sun	|2,1,1>	2	1	1	1	0	27	2	(|m|+1) / |m|	n'-1	12.50	13.5	2*6^1=	12	2.25

Example-6: For Saturn surface's fast-flow streams |3,2,2> and |3,2,1>, determine the residue nLL QM state's |m| and n' value.

In SunQM-3s3's Fig-7 (that copied here as Figure 3a and Figure 3b), Saturn's fast-flow equatorial zonal band was assigned to be the residue |3,2,2> QM state. According to wiki "Saturn", Saturn's equatorial rotation velocity is 9.87 km/s. According to [39] (see Figure 3c), the residue |3,2,2> zonal band is (read as) ~ 470 m/s faster than Saturn ball's equatorial rotation (background) velocity 9870 m/s. Using the same method in Example-5 (for Jupiter's |5,4,4> zonal band), we have $\frac{+|m|+1}{+|m|} = \frac{v_{faster}}{v_{normal}} = \frac{9870+470}{9870}$, |m| ≈ 21 , n = |m| + 1 ≈ 22. At Saturn's surface equator, the residue |3,2,2> QM state should have either n = 3, or n' = 3*3^1 = 9, or n' = 3*3^2 = 27, etc. After an approximation, I chose n'= 3*3^2 = 27 for the positive precession of the residue |3,2,2> QM state stream, that will be $\frac{27}{26} = \frac{9870+x}{9870}$, x ≈ 379.6 m/s faster than the background 9870 m/s. It reasonably well matches the observed ~ 470 m/s speed.

For Saturn's |3,2,1> band (see in Figure 3b) at θ' ≈ 30° latitude region, Saturn ball's rotation (background) velocity at θ' ≈ 30° is cos(30°) * 9870 m/s ≈ 8548 m/s. From Figure 3c, |3,2,1> band is (read as) ~ 150 m/s faster than that of the background speed (8548 m/s). Using the same method in Example-5 (for Jupiter's |5,4,3> fast zonal band), we have $\frac{+|m|+2}{+|m|} = \frac{v_{faster}}{v_{normal}} = \frac{8548+150}{8548}$, |m| ≈ 114 , n' = |m| + 2 ≈ 116. At Saturn surface, the residue |3,2,1> QM state should have either n = 3, or n' = 3*3^3 = 81, or n' = 3*3^4 = 243, etc. After an approximation, I chose n' = 3*3^3 = 81, for the positive precession of the residue |3,2,1> QM state stream, that will be $\frac{81}{79} = \frac{8548+x}{8548}$, x ≈ 216.4 m/s faster than the background 8548 m/s. It reasonably well matches the observed ~150 m/s speed. All above results were list in Table 2.

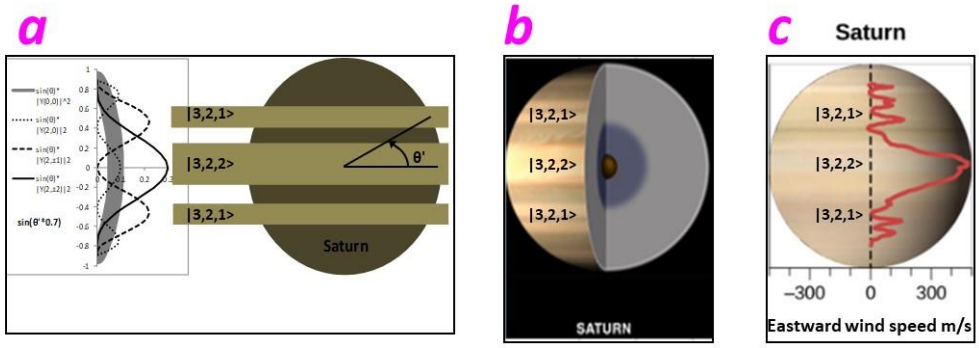

Figure 3a. For |3,2,m> QM states, to correlate the latitude positions between the calculated Born probability peaks and the observed Saturn surface's zonal bands (see Figure 3b). Copied from SunQM-3s3's Fig-7a.

Figure 3b. Idealized illustration of Saturn surface's zonal bands. Copied from wiki "Planetary core" figure "The internal structure of the outer planets". Author: Lunar and Planetary Institute - https://solarsystem.nasa.gov/galleries/gas-giant-interiors. Copyright: Public Domain. Also shown in SunQM-3s3's Fig-7c, and analyzed as |3,2,m> by me.
Figure 3c. Zonal wind speeds in the atmosphere of Saturn. Copied from [39]. Assigned as the |3,2,m> QM state by me.

Example-7: For Earth's polar jet at residue |4,3,1> , determine the residue nLL QM state's |m| and n' value.

As wiki "Jet stream" explained, "*Jet streams are fast flowing, narrow, meandering air currents in the atmospheres*" of Earth. The (stronger) polar jets locate at ~60° latitude and 9 ~ 12 km above sea level, and the (weaker) subtropical jets locate at ~30° latitude and 10 ~ 16 km above sea level. In SunQM-3s6, I toke Earth core as the size of p{0,1//2} with $r_1 = r_{Earth\text{-}core}$, then Earth's mantle shell is in p{0,1//2}o orbital shell with n = 1. (Note: in SunQM-4s2's Fig-3, I assigned the Earth atmosphere shell as the effective p{0,2//2}o orbital shell of the Earth. Then, assigned the Polar jet and the Subtropical jet as the residue |3,2,0> and |3,2,1> QM states. Now I think that is incorrect). Here (in Figure 4), I re-assigned the polar jet as in |4,3,1> QM state, the subtropical jets as in |4,3,2> QM state. For this, I have to re-assign the Earth atmosphere shell as the effective p{0,3//2}o orbital shell of the Earth, and assign the Earth crust shell as the effective p{0,2//2}o orbital shell of the Earth. Wiki "Jet stream" mentioned that "*The polar jet stream can travel at speeds greater than 180 km/h*", that is, 50 m/s faster than the Earth body's rotation (background) speed 233 m/s at 60° latitude (calculated as: Earth's equatorial rotation speed 465 m/s (see wiki "Earth") times cos(60°) = 233 m/s, and suppose the Earth atmosphere's speed at 60° latitude is the same as that the ground speed). Then, for the Polar jet stream's residue |4,3,1> QM state, we have $\frac{+|m|+3}{+|m|} = \frac{233+50}{233}$, |m| ≈ 14, n' = |m| + 3 ≈ 17. At Earth atmosphere outer edge, the residue |4,3,1> QM state should have either n = 4, or n' = 4*4^1= 16, etc. After an approximation, I chose n' = 4*4^1 = 16, for the positive precession of the residue |4,3,1> QM state for the polar jet stream. It will be $\frac{16}{13} = \frac{233+x}{233}$, x ≈ 54 m/s faster than the background 233 m/s. It well matches the observed ~ 50 m/s speed. This result was list in Table 2.

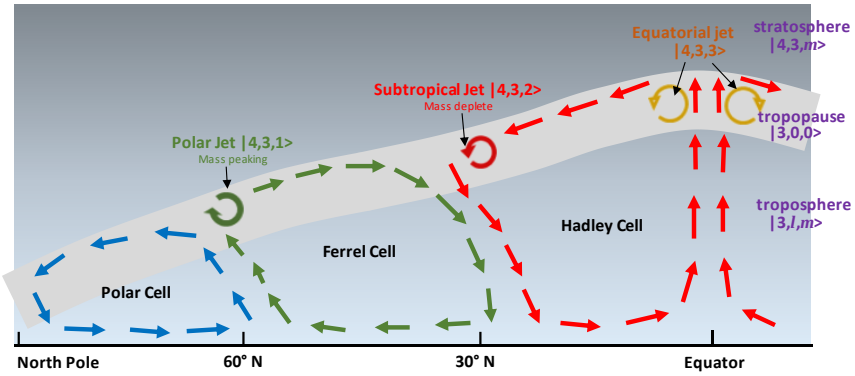

Figure 4. Cross section of the subtropical and polar jet streams by latitude, explained with {N,n} QM analysis. Copied and corrected from SunQM-4s2's Fig-3. It was drawn based on wiki "Jet stream" figure "Cross section of the subtropical and polar jet streams by latitude" with many modifications.

Example-8: Treat Sun's equatorial fast-flow region as the residue |2,1,1> QM state, determine the |m| and n' value of the positive precession relative to the Sun body's background rotation speed at the |1,0,0> QM state.

The {N,n} QM structure of the Sun contains a core at the size of {0,1//6}, and a {0,1//6}o orbital shell with size of {0,2//6}. Although the mass in Sun's {0,1//6}o orbital shell is in |1,0,0> QM state, on the surface equator, there should be some small amount of mass is in the residue |2,1,1> QM state. According to wiki "Sun" (and also see Figure 1b), Sun's sidereal rotation has 25.05 days at equator (with equatorial rotation velocity 1997 m/s), and 34.4 days at poles. After an approximation, I chose 25 days as the speed for the faster equatorial rotation region that is in the residue |2,1,1> QM state, and chose 27 days as the speed for the background (normal, or relatively slower) rotation region that in the |1,0,0> QM state.

Then, using the same method in Example-5 (for Jupiter's |5,4,4> fast zonal band), we have $\frac{+|m|+1}{+|m|} = \frac{T_{normal}}{T_{faster}} = \frac{27}{25}$, |m| = 12.5, n' = |m| + 1 = 13.5. At Sun's surface equator, the residue |2,1,1> QM state should have either n = 2, or n' = 2*6^1=12, or n' = 2*6^2=72, etc. After an approximation, I chose n' = 12, for the positive precession of the residue |2,1,1> QM state stream, that will be $\frac{12}{11} = \frac{T_{normal}}{T_{faster}} = \frac{27}{T_{faster}}$, T_{faster} = 24.75 days relative to the normal 27 days period. It reasonably well matches the observed 25 days fast equatorial period.

In Table 2, I listed the results for all above examples, and showed that the residue nLL QM state (under the chosen n') caused positive precession speeds (in the yellow cells) do reasonably match to the observed speeds of the fast zonal band streams (in the green cells) for all listed celestial bodies.

III. A (minor) part of this residue nLL QM state's positive precession may can further be developed as a +/- |m| cycle, and then it can be used to explain the Y*l*m cycle (like in the sunspot drift, continental drift, etc.)

The unexpected positive precession from the pure QM deduction (in eq-4) made me to further guess that, if there exists a cycle of positive precession and negative precession (in QM), then I may able to use it to explain the Y*l*m cycle for both the sunspot drift on the Sun surface, and the continental drift on the Earth (mantle) surface (see SunQM-3s9, notice that both drifts are in the residue nLL QM states). Furthermore, if it exists a cycle of positive/negative precession (in QM), then I may be able to use it to explain the acceleration/deceleration cycle of the elliptical orbital motion of the planets around the Sun. Then how to derive out a cycle of positive/negative precession out of the eq-4 (that apparently only shows a positive precession)? After several years of work (since March 2020), I figured out one possible way, and showed it in the current section.

III-a. The simultaneous +|m| and -|m| quantum number motions of the |n,*l*,m> QM state (that described by the Schrodinger equation) may become the "face-opposite-face locked binary orbital motion" in φ-1D bi-direction, then transformed to be a θ-1D orbital uni-directional motion with half-period +|m| and half-period -|m|

In the QM text books [40] ~ [42], solving the Schrodinger equation (for the hydrogen atom) generated the QM state of |n,*l*,m>, where for each n state, *l* = 0, 1, … (n-1), and m = -*l*, … +*l*. Similarly, solving the Schrodinger equation for the Solar system gave the same result as that of the hydrogen atom (see SunQM-3 series). Figure 5a illustrated the vector model of an orbital angular momentum at *l* = 2 that with m = -2, -1, 0, 1, 2. Notice that for a macro-world system with ~100% mass occupancy, (e.g., inside a Sun with 100% mass occupancy), for each **n state** and for each ***l* sub-state**, all +/- valued **m sub-sub-states** are co-existing. To simplify the analysis, here I only mention one pair of the +/- valued m at the nLL QM state, and ignore the rest m states in between. (Note: Here I often use "±m", rather than the more accurate "±|m|" to represent the +/- valued pairs of m quantum number). For example, for the |n,*l*,±m> = |3,2,±2> QM nLL states, their Schrodinger equation's solutions (i.e., the NBP, or the Y(*l*,*m*) wave function, as shown in wiki "Table of spherical harmonics") in θφ-2D are

$$Y(l=2, m=+2) = \frac{1}{4}\sqrt{\frac{15}{2\pi}} e^{im\varphi} \sin^2\theta = \frac{1}{4}\sqrt{\frac{15}{2\pi}} e^{i2\varphi} \sin^2\theta \qquad \text{eq-9a}$$

and,

$$Y(l=2, m=-2) = \frac{1}{4}\sqrt{\frac{15}{2\pi}} e^{im\varphi} \sin^2\theta = \frac{1}{4}\sqrt{\frac{15}{2\pi}} e^{-i2\varphi} \sin^2\theta \qquad \text{eq-9b}$$

From them, I guessed that these two waves (or wave functions, or NBPs, both in nLL QM state) with m = ±2 should be doing orbital rotation in φ-1D in the opposite directions (meaning, simultaneously one in +φ direction and another one in -φ

direction). However, at first, I did not fully understand how this works in a real physical world in the particle view (although I did understand the standing wave view (for matter wave's phase wave)). Then, after the study in SunQM-6s7, I finally figured out that "*For a pair of spin up/down electrons, their (…) orbital movement in φ-1D (in the opposite ±φ directions) may have transformed into a uni-directional orbital movement in θ-1D*". Also, in SunQM-6s10, I figured out the similar result that "*A ^{4}He nucleus is constituted with two same neutron-proton binaries that are doing the "face-to-face plus face-opposite-face two-level orbital motion". Within each one binary, the neutron and proton are doing the "face-to-face tidal-locked orbital binary motion" with the parallel nuclear spin ⇑⇑↑. Between the two binaries, they are doing the "face-opposite-face locked binary orbital motion" in φ-1D bi-direction with the anti-parallel nuclear spin ⇑⇑↑⇓⇓↓, that eventually transformed to be a θ-1D orbital uni-directional motion*". (Note: for the detailed explanation, see SunQM-6s7's Fig-5b and Fig-5c, and see SunQM-6s10's Fig-1c and Fig-1d).

Based on the above new knowledge, now I believed that we can treat the superpositioned m = ±2 states (in Figure 5a) as the two virtual angular momentum vectors ($\vec{L}_{\pm z}$) in φ-1D, one at φ = 0 position with the $\vec{L}_{+z}$ upward (that equivalent to He-atom's n = 1 electron with spin-up), and the second one at either φ = 0 or π position (or at any φ position, see Appendix A) with the $\vec{L}_{-z}$ downward (that equivalent to He-atom's n = 1 electron with spin-down, as shown in SunQM-6s7's Fig-5b). (It can be treated as that) they are doing the virtual circular orbital motion in φ-1D, but one in +φ direction, another in -φ direction, simultaneously (or, we call it "φ-1D bi-direction motion"). Then, this "φ-1D bi-direction motion" is transformed into (or equivalent to) a single virtual angular momentum vector $\vec{L}_{\theta}$ that is doing the "θ-1D uni-directional motion" (as shown in Figure 5b, and also shown in SunQM-6s7's Fig-5c). Then, according to Figure 5a, during its "θ-1D uni-directional motion", the virtual vector $\vec{L}_{\theta}$ in Figure 5b has half-cycle in the +|m| region (e.g., θ = +0.5π → 0π → -0.5π), and second half-cycle in the -|m| region (e.g., θ = -0.5π → -π → -1.5π). Note: Check Appendix A for a more complicated explanation for Figure 5. Note: Does half-cycle +|m| plus half-cycle -|m| looks like a Mobius strip?

Furthermore, I believed that the two superpositioned m = ±2 QM states (that solved from the Schrodinger equation, and represented by the two virtual angular momentum vectors $\vec{L}_{\pm z}$, and thus represented by the two oppositely moving waves in φ-1D) are the two "phase waves" that are doing the ±φ directional motion in the φ-1D (for simplicity, let's assuming that it is in the nLL state). They are not the "group waves" (because for nLL state, the group wave has to be a single wave packet that is doing uni-direction motion in the φ-1D).

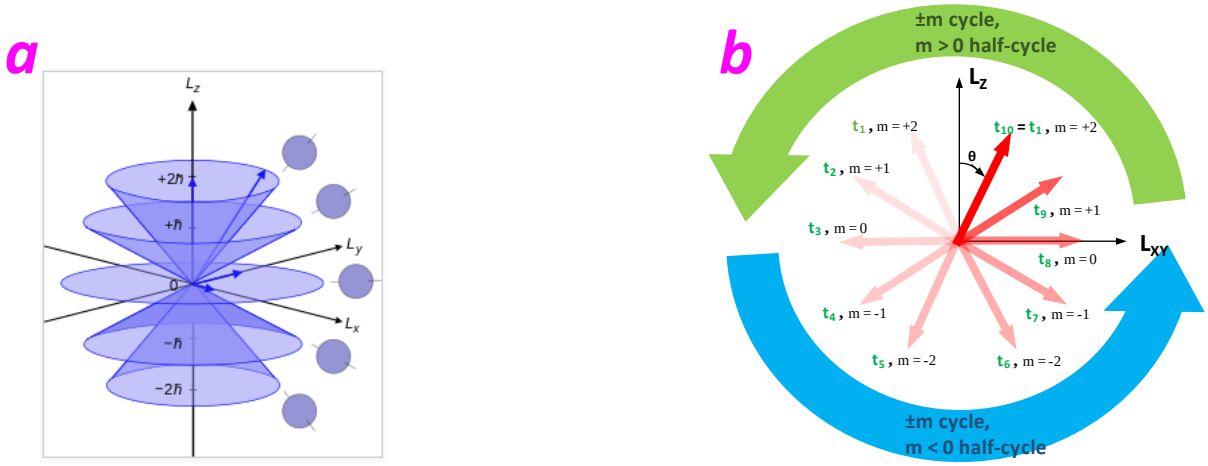

Figure 5a. Illustration of the vector model of orbital angular momentum for the |n,*l*,m> = |3,2,m> QM states. Copied from wiki "Angular momentum operator". Author: Maschen. Copyright: Public Domain.

Figure 5b. To illustrate that the two superpositioned m = ±2 QM states (in Figure 5a) may can be treated as the two virtual angular momentum vectors ($\vec{L}_{\pm z}$) that are doing the "φ-1D bi-direction motion" head-to-head, and then transformed into a "θ-1D uni-direction motion". (Note: See SunQM-6s7's Fig-5b, and SunQM-6s7's Fig-5c for better understanding). Then, it forms a ±m cycle with half-cycle at m > 0, and half-cycle at m < 0.

III-b. The +|m| QM state may produce a positive precession for the (minor) residue nLL QM state stream, and the -|m| QM state may produce a negative precession for the same (minor) residue nLL QM state stream

Then, the next question is, how to link this ±m (or ±φ) motion to the eq-6 (that in eq-4)? For nLL QM state, with half period of +|m|, and half period of -|m|, eq-6 and eq-7 can be re-written as

$$\frac{m+1}{m}\omega_n = \begin{cases} \frac{+|m|+1}{+|m|}\omega_n = \frac{|m|+1}{|m|}\omega_n > \omega_n, & when\ m\ = +|m| \\ \frac{-|m|+1}{-|m|}\omega_n = \frac{|m|-1}{|m|}\omega_n\ < \omega_n, & when\ m\ = -|m| \end{cases} \qquad \text{eq-10}$$

The physical meaning of eq-10 is, when the quantum number m is a positive value, eq-10 becomes a positive precession for the residue nLL QM state; when m is a negative value, the same eq-10 becomes a negative precession for the residue nLL QM state. Therefore, for the (minor) residue nLL QM state, the apparent positive-precession-only formula (in eq-4) now becomes a cycle of positive/negative precession (in eq-10).

Furthermore, for eq-10, I still assumed that eq-8 is still valid for the +|m| half-period. Although for the -|m| half-period, eq-8 becomes

$$\frac{n'}{n'-1} = \frac{-|m|+1}{-|m|} = \frac{v_{slower}}{v_{normal}} = \frac{1/T_{slower}}{1/T_{normal}} = \frac{T_{normal}}{T_{slower}} \qquad \text{eq-11}$$

Notice that the new ±m cycle caused positive/negative precession cycle is on top of the real angular momentum vector $\vec{L}_{+z}$ nLL orbital motion. Therefore, the positive/negative precession is the minor effect relative to the (major) $\vec{L}_{+z}$ nLL orbital motion. Thus, this positive/negative precession cycle belongs to the minor residue nLL state, while the major residue nLL state keeps a constant positive precession. Because the $\vec{L}_{+z}$ nLL orbital motion has its own period, and the positive/negative precession cycle may also have its own period, these two period may be equal to each other (see example in the section III-c), or they may be not equal to each other (see example in the section III-d).

Note: eq-10 fully support Babcock's magnetic dynamo model [37]. That is, in the second phase of Y*l*m cycle, the equatorial fast-flow stream simply turned into a slow-flow stream. Thus, my previous explanation for the second phase of Y*l*m cycle in SunQM-3s9's section-I-e (or in SunQM-3s9's Fig-2) is unnecessary, or may even be incorrect.

III-c. When the period of the positive/negative precession cycle equals to the period of the $\vec{L}_{+z}$ nLL orbital motion, it will show up as a (perfect) elliptical orbital motion for a nLL QM state with half-period acceleration and half-period deceleration

In Figure 6, for an elliptical orbital motion in xy-plane with the aphelion on the +y axis and the perihelion on the -y axis, the (green colored) orbital motion from +y axis to -x axis to -y axis is in the acceleration phase, and it equals to the positive-precession that caused by the virtual vector ($\vec{L}_{\theta}$)'s θ-1D uni-directional motion of ±m cycle at the +|m| half-cycle (at θ = +0.5π → 0π → -0.5π, see the green half-cycle motion in Figure 5b). In contrast, the (blue colored) orbital motion from -y axis to +x axis to +y axis is in the deceleration phase, and it equals to the negative-precession that caused by the virtual vector ($\vec{L}_{\theta}$)'s θ-1D uni-direction motion of ±m cycle at the -|m| half-cycle (at θ = -0.5π → -π → -1.5π, see the blue half-cycle motion in Figure 5b). Question: Can we say that nLL only causes circular orbital motion, the residue nLL modifies the circular orbit to be an elliptic orbit?

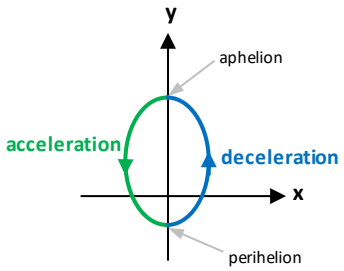

Figure 6. An elliptical orbital motion has half-cycle in acceleration and half-cycle in deceleration.

Example-9: From Earth elliptical orbit's eccentricity, to estimate the |m| = n-1 value for this elliptical orbit.

According to wiki "Elliptic orbit", when orbiting the Sun, Earth has the elliptical orbital speed:

$$v = \sqrt{GM\left(\frac{2}{r} - \frac{1}{a}\right)} \qquad \text{eq-12}$$

where M is the reduced mass of Sun and Earth, r is the distance between Earth and Sun, *a* is the length of the semi-major axis of Earth's elliptical orbit around Sun. Thus, the elliptical orbital speed at the aphelion is:

$$v_{ap} = \sqrt{GM\left(\frac{2}{a(1+e)} - \frac{1}{a}\right)} \qquad \text{eq-13}$$

where eccentricity $e = c/a$, $c^2 = a^2 - b^2$, b is the length of the semi-minor axis, $r_{aphelion} = a + c = a + ea = a(1+e)$. Also, the elliptical orbital speed at the perihelion (where $r_{perihelion} = a - c = a - ea = a(1-e)$) is:

$$v_{peri} = \sqrt{GM\left(\frac{2}{a(1-e)} - \frac{1}{a}\right)} \qquad \text{eq-14}$$

Then

$$\frac{v_{peri}}{v_{ap}} = \sqrt{GM\left(\frac{2}{a(1-e)} - \frac{1}{a}\right)} \Big/ \sqrt{GM\left(\frac{2}{a(1+e)} - \frac{1}{a}\right)} = \frac{1+e}{1-e} \qquad \text{eq-15}$$

From eq-10, (using a citizen scientist leveled approximation), we may can treat the maximum positive precession speed v_{peri} (at the perihelion) equivalents to $\frac{|m|+1}{|m|}\omega_n r$, and treat the maximum negative precession speed v_{ap} (at the aphelion) equivalents to $\frac{|m|-1}{|m|}\omega_n r$, where r is the (near) circular orbit radius. Then,

$$\frac{v_{peri}}{v_{ap}} = \left(\frac{|m|+1}{|m|}\omega_n r\right) \Big/ \left[\frac{|m|-1}{|m|}\omega_n r\right] = \frac{|m|+1}{|m|-1} \qquad \text{eq-16}$$

Then, we have eq-15 equals to eq-16,

$$\frac{1+e}{1-e} = \frac{|m|+1}{|m|-1}, \; or, \; |m| = \frac{1}{e} \qquad \text{eq-17}$$

According to eq-17, for the planet Earth's elliptic orbit with $e = 0.017$, its $|m| = 1/e \approx 59$, n' = |m| + 1 ≈ 60. For Earth's orbit at {1,5//6}, the high-frequency can be n' = 5*6^1 = 30, 5*6^2 = 180, etc., and with |m| = L = n - 1. Thus, (as

shown in Table 3), choosing n' = 30 (or |the residue |30,29,29> QM state with {0,1//6} as r_1) as the residue nLL state will best match Earth's elliptic orbit with e = 0.017.

As shown in Table 3, the similar calculations have been applied to all planets (and even the Moon) in the Solar system. For example, Venus's elliptic orbit with e = 0.007, it has |m| ≈ 143, n' ≈ 144, and then choosing n' = 4*6^2 = 144 (with {-1,1//6} as r_1) will best match this eccentricity; Mercury's elliptic orbit with e = 0.205, it has |m| ≈ 4.9, n' ≈ 5.9, and then choosing n' = 3 (with {1,1//6} as r_1) will best match this eccentricity, etc. All these results suggested that the eccentricity of a planet/moon's elliptic orbit may can be described (or, at least partly described) by the positive/negative precession cycle of the (minor) residue nLL QM state.

Table 3. Using eccentricity value to estimate the |m| = n-1 value for the elliptic orbit for all planets/moons.

NASA data	MERCURY	VENUS	EARTH	MARS	JUPITER	SATURN	URANUS	NEPTUNE	PLUTO		MOON
Mass (1024kg)	0.33	4.87	5.97	0.642	1898	568	86.8	102	0.0146		0.073
Distance from Sun (106 km)	57.9	108.2	149.6	227.9	778.6	1433.5	2872.5	4495.1	5906.4		0.384*
Perihelion (106 km)	46	107.5	147.1	206.6	740.5	1352.6	2741.3	4444.5	4436.8		0.363*
Aphelion (106 km)	69.8	108.9	152.1	249.2	816.6	1514.5	3003.6	4545.7	7375.9		0.406*
Orbital Period (days)	88	224.7	365.2	687	4331	10,747	30,589	59,800	90,560		27.3
Orbital Velocity (km/s)	47.4	35	29.8	24.1	13.1	9.7	6.8	5.4	4.7		1
Orbital Eccentricity	***0.205***	***0.007***	***0.017***	***0.094***	***0.049***	***0.057***	***0.046***	***0.011***	***0.244***		***0.055***
Estimation for nLL											
|m|= 1/e	4.9	142.9	58.8	10.6	20.4	17.5	21.7	90.9	4.1		18.2
n= |m|+1	5.9	143.9	59.8	11.6	21.4	18.5	22.7	91.9	5.1		19.2
Chose nLL QM state											
{-1,1//6} = r_1	108	144	180	216	432	648	864	1080	1296	{0,1//2} = r_1	1
{0,1//6} = r_1	18	24	30	36	72	108	144	180	216	{1,1//2} = r_1	2
{1,1//6} = r_1	3	4	5	6	12	18	24	30	36	{2,1//2} = r_1	4
{2,1//6} = r_1					2	3	4	5	6	{3,1//2} = r_1	8
										{4,1//2} = r_1	16

Note: Data in rows 1~8 were obtained from (http://nssdc.gsfc.nasa.gov/planetary/factsheet/).

III-d. When the period of the positive/negative precession cycle is much longer than the period of the $\vec{L}_{+z}$ nLL orbital motion, it will show up as an Y*l*m-cycled orbital motion (for a minor residue nLL QM state stream) with many rounds of positive precession followed by many rounds of negative precession (like that in the sunspot drift and the continental drift)

In SunQM-3s9, based on Babcock's magnetic dynamo model [37], and also based on the {N,n//q} QM structure, I had proposed an Y*l*m cycle model to explain the 22 years period cycle of the sunspot drift. Now, with the new knowledge learned in this paper, I need to modify this model. An Y*l*m cycle contains two phases. In phase-1 of the Y*l*m cycle, the nLL QM force induces the mass peaking and upwelling effect below the surface of an {N,n}o orbit shell, and generates an equatorial fast-flow stream at the surface (that correlates to the +|m| caused positive precession). As phase-1 progress, the equatorial fast-flow stream gets narrower and shallower and slower (as the n number of the nLL getting larger and larger), and eventually diminished (to the normal-flow background). In the phase-2 of the Y*l*m cycle, the nLL QM force also induces the mass peaking and upwelling effect below the surface of an {N,n}o orbit shell, but generates an equatorial slow-flow stream at the surface (that correlates to the -|m| caused negative precession). As phase-2 progress, the equatorial slow-flow stream gets narrower and shallower and faster (as the n number of nLL getting larger and larger), and eventually diminished (to the normal-flow background). This Y*l*m cycle model not only well matches to Babcock's model, but also described in a pure QM version. It can be used to explain the sunspot drift on Sun surface, the continental drift on Earth surface, and both Sun's and Earth's magnetic dynamo. The alternation between two phases of Y*l*m cycle not only alternates the orientation of Sun's (or Earth's) magnetic field, but also supports the supercontinent cycle model (because so far, the supercontinent cycle is only a guessed model).

Example-10: Assuming the 22 years period cycle of the sunspot drift is caused by the +/- |m| cycle of the (minor) residue |2,1,1> QM state (i.e., the Y*l*m cycle) in the Sun, let's determine the |m| value for this residue |2,1,1>.

As shown in Example-8, Sun's equatorial rotation velocity (that is the major residue |2,1,1> QM state fast-flow stream) is 1997 m/s. In SunQM-3s9, the preliminary estimation showed that the sunspot stream may be 20 m/s ~ 100 m/s faster than the background speed 1997 m/s. Let's pick that it is ~ 100 m/s faster. Notice that this speed is not a constant speed, it is more like a cycle that gradually increased from 0 m/s faster to 100 m/s faster, then gradually decreased to -100 m/s, then gradually back to 0 m/s faster. For the purpose of determining the |m|, I simplified this process as that it is constantly 100 m/s faster in the +|m| half-period, and constantly -100 m/s slower in the -|m| half-period. Then, using eq-8 and eq-11, we have $\frac{+|m|+1}{+|m|}=\frac{v_{faster}}{v_{normal}}=\frac{1997+100}{1997}$, |m| ≈ 20, n' = |m| + 1 ≈ 21, and $\frac{-|m|+1}{-|m|}=\frac{v_{slower}}{v_{normal}}=\frac{1997-100}{1997}$, |m| ≈ 20, n = |m| + 1 ≈ 21. At Sun's surface equator, the residue |2,1,1> QM state should have either n = 2, or n' = 2*6^1=12, or n' = 2*6^2=72, etc. As shown in Table 4, if I chose n' = 12, m = n - 1 = 11, for the positive precession of the minor residue |2,1,1> QM state stream, that will be $\frac{12}{11}=\frac{1997+x}{1997}$, x ≈ 181.5 m/s faster (or slower) than the background 1997 m/s. However, if I chose n' = 2*6^2 = 72, or 2*6^3 = 432, the calculated fast-flow speed will become 28.1 m/s, or 4.6 m/s. These results revealed that, as the Y*l*m cycle progressing, if the n' (of the minor residue nLL state) is increasing, then the minor residue nLL fast-flow stream become slower.

Note: Sun has a major (steady state) residue |2,1,1> stream (with the fixed n = 2, with the constant equatorial speed 1997 m/s, and with more than 90% of the mass in the residue |2,1,1> state), and a minor (cyclic) residue |2,1,1> stream (with the variable n increasing from 2 to infinity, with the variable equatorial speed 1997±100 m/s, and with less than 10% of the mass in the residue |2,1,1> state). It is the minor residue |2,1,1> stream that forms the Y*l*m cycle that caused the sunspot and the drifting of sunspot. In this case, although the speed of the minor residue |2,1,1> stream (1997±100 m/s) is not too different than the background |1,0,0> speed at the surface equator (1997 m/s), but the period of the residue |2,1,1> stream's +/- |m| cycle is 22 years, much longer than the spin-period of Sun surface equator (~25 days, as the constant background relative to the Y*l*m cyclic stream).

Table 4. For sunspot drift's minor residue |2,1,1> QM state in an Y*l*m cycle, higher n' will cause slower flow speed.

n'=2*6^	pick n'=	speed faster
		m/s
=2*6^1	12	181.5
=2*6^2	72	28.1
=2*6^3	432	4.6

Example-11: Assuming Earth's continental drift is caused by the +/- |m| cycle (or the Y*l*m cycle) of the mantle's (minor) residue |2,1,1> QM state, let's determine the |m| value for this residue |2,1,1>.

The Pangaea supercontinent was formed more than ~300 Mya (millions years ago, see wiki "Pangaea"). and (according to wiki "supercontinent cycle") let's assume that it is caused by an Y*l*m cycle with period of 500 million years (relative to Earth spin period one day = 1/365 year). Thus, with the (faster-period) = 500,000,000 - 1/365 years, and (normal-period) = 500,000,000 years, $\frac{+|m|+1}{+|m|}=\frac{T_{normal}}{T_{faster}}=\frac{500000000}{(500000000-1/365)}$, |m| ≈ 1.825E+11, n' = |m| + 1 ≈ 1.825E+11. Under the Earth's {N,n//2} QM structure, at Earth mantle's outer edge, the residue |2,1,1> QM state should have either n = 2, or n' = 2*2^10 = 2048, or n' = 2*2^36 = 1.374E+11, etc. After an approximation, I chose n' = 2*2^36 = 1.37438953472E+11, m = n - 1 = 2*2^36 = 1.37438953471E+11. This means, for the Earth mantle's outer edge's (base-frequency) residue |2,1,1> QM state, it developed a (high-frequency) n'= 2*2^36, or a (high-frequency) minor residue nLL QM state of |1.37438953472E+11, 1.37438953471E+11, 1.37438953471E+11> with positive/negative precession cycle (only 1/365 year shorter than the 500,000,000 years period). Then, the back calculation $\frac{+|m|+1}{+|m|}=\frac{T_{normal}}{T_{faster}}$ gives $\frac{137438953472}{137438953471}=\frac{x}{x-1/365}$, x ≈ 376E+6 years. Thus, at n' = 2*2^36, a (high-frequency) minor residue nLL QM state caused the Earth's continental drift with an Y*l*m cycle period of 376 million years (reasonably close to 500E+6 years).

If we choose different n', then the calculated Y*l*m cycle period will be different (see in Table 5). Wiki "Supercontinent" listed some possible ancient supercontinents (Ma = millions of years ago): Vaalbara (3,636–2,803 Ma), Ur (2,803–2,408 Ma), Kenorland (2,720–2,114 Ma), Arctica (2,114–1,995 Ma), Atlantica (1,991–1,124 Ma), Columbia (Nuna) (1,820–1,350 Ma), Rodinia (1,130–750 Ma), Pannotia (633–573 Ma), Gondwana (550–175 Ma), Pangaea (336–175 Ma).

According to their period, and checking on Table 5, we may can determine that each ancient supercontinent was caused by what n' of the minor residue nLL stream's Y*l*m cycle.

Table 5. For Earth's {N,n//2} QM structure caused minor residue nLL Y*l*m cycles, different n' will cause different period.

pick n'=2*2^N	pick n'=	Ylm cycle period
N=		years
10	2048	5.608E+00
30	2.14748364800E+09	5.880E+06
31	4.29496729600E+09	1.176E+07
32	8.58993459200E+09	2.352E+07
33	1.71798691840E+10	4.704E+07
34	3.43597383680E+10	9.408E+07
35	6.87194767360E+10	1.882E+08
36	1.37438953472E+11	3.763E+08
37	2.74877906944E+11	7.527E+08

Example-12: Assuming the slow-flow stream at the middle of Jupiter's |5,4,4> zonal band is caused by the negative precession of an Y*l*m cycle, determine the |m| and n' for this Y*l*m cycle.

See in Figure 2c, Jupiter's main zonal band |5,4,4> (that within θ' ≈ ±20° latitude range) approximately has the equatorial velocity of ~130 m/s faster than the background equatorial rotation velocity 12.6 km/s, while the middle minor slow-flow stream (that within θ' ≈ ±3° latitude range) only has the equatorial velocity of ~70 m/s faster than the background equatorial rotation velocity 12.6 km/s. $\frac{-|m|+1}{-|m|}=\frac{v_{slower}}{v_{normal}}=\frac{12600+70}{12600+130}$, |m| ≈ 212. If I choose n'= 5*5^2 = 125, m = n - 1 = 124, that will be $\frac{-|m|+1}{-|m|}=\frac{-123}{-124}=\frac{12600+x}{12600+130}$, x ≈ 27.3 m/s faster than the background 12600 m/s, or 130 – 27 = 103 m/s slower than the major residue |5,4,4> fast-flow stream at 130 m/s. If I choose n'= 5*5^3 = 625, m = n - 1 ≈ 624, then this minor residue |5,4,4> will be ~110 m/s faster than the background 12600 m/s, or ~ 20 m/s slower than the major residue |5,4,4> fast-flow stream at 130 m/s.

Example-13: Assuming the slow-flow stream at the middle of Saturn's |3,2,1> fast-flow zonal band is caused by the negative precession of an Y*l*m cycle, determine the |m| and n' for this Y*l*m cycle.

As shown in the Example-6, for Saturn |3,2,1> band at θ' ≈ 30°, Saturn ball's rotation local velocity is cos(30°) * 9870 m/s ≈ 8548 m/s. From Figure 3c, |3,2,1> band (that within θ' ≈ 30°±10° latitude range in Figure 3b, here we only using the northern |3,2,1> band as the example) is ~ 150 m/s faster than that of the background speed (8548 m/s), and the |3,2,1> negative precession band (that within θ' ≈ 30°±1° latitude range in Figure 3b) is ~ 0 m/s faster than that of the background speed (8548 +150 m/s). $\frac{-|m|+2}{-|m|}=\frac{v_{slower}}{v_{normal}}=\frac{8548+0}{8548+150}$, |m| ≈ 116, n' = |m| + 2 ≈ 118. At Saturn surface, for the possible minor residue |3,2,1> QM state's high-frequencies, I chose n'= 3*3^3 = 81, m = n - 2 ≈ 79. Then, $\frac{-|m|+2}{-|m|}=\frac{-77}{-79}=\frac{8548+x}{8548+150}$, x ≈ -70 m/s. This means, at the middle of a fast-flow stream of Saturn's 30°±10° latitude region (that caused by the major residue |3,2,1> QM state, with speed at 8548 +150 m/s), a minor residue |3,2,1> state (within θ' ≈ 30°±1° latitude range) produced a minor slow-flow steam (at speed of 8548 -70 m/s).

IV. Will Mercury perihelion positive precession become a negative precession in the future? And/or, does it exist multiple levels of Y*l*m cycle (with multiple periods)?

The major residue nLL QM state is described to have only the positive precession (as shown in section-I and section-II), while the minor residue nLL QM state is described to have the positive/negative precession cycle (as shown in section-III). However, is it possible that all the positive-only precession QM process (that derived from the QM process in eq-4, and shown in the section-I and section-II) are actually also the positive/negative precession cycle (but with a much longer cycle period)? If this is correct, then,

1) For the Mercury's perihelion precession, it (the residue nLL QM state) may be currently in the positive precession half-cycle (of a whole Y*l*m cycle). Sometime in the future, Mercury's perihelion precession may will become a negative precession, (and this would apply to all other planets' orbital precession).
2) Similarly, for Jupiter surface atmosphere's fast-flow zonal bands (in the major residue nLL or |5,4,m> QM state), they may be currently also in the positive precession half-cycle (of the whole Y*l*m cycle). Sometime in the future, these |5,4,m> QM state zonal bands may will become slow-flow bands on Jupiter surface, (and this would apply to all other planets' surface atmospheric zonal bands).
3) Why this is possible? In {N,n} QM, we said that the Earth's continental drift is currently in the positive precession half-cycle of a whole Y*l*m cycle, mainly because the geological evidences suggested that there might have multiple continental cycles in the Earth's geological history. If without those geological evidences, with the extreme long period of the Y*l*m cycle (greater than 10^5 years?), we can only say that the Earth's continental drift is a positive-only precession (that is described by eq-4), and this is just like that we see the current Mercury's perihelion precession is a positive-only precession, and current Jupiter's fast-flow zonal band is a positive-only precession.
4) If the above explanation is correct, then, the only difference between the minor and the major residue nLL QM state is, the minor residue nLL has a short period of Y*l*m cycle, while the major residue nLL has a long period of Y*l*m cycle. Furthermore, for each residue nLL QM state, there may have multiple levels of Y*l*m cycles with multiple periods.
5) Why currently all planets' orbital perihelion precession are in the positive precession, and all planets' surface zonal bands are in positive precession, and Earth's continental drift is also in positive precession? Maybe they are all correlated with each other in the Solar system, and the Solar system (as a whole) is currently in the positive precession half-cycle (of a whole Y*l*m cycle). Maybe sometime in the future, the Solar system (as a whole) move to the negative precession half-cycle (of the whole Y*l*m cycle), and then all these precessions will become negative.
6) Furthermore, for each celestial body, it may exist many levels of residue nLL QM state caused positive precessions (or positive/negative precession cycles, or Y*l*m cycles). Take Jupiter as the example: Jupiter's minor residue |5,4,4> QM state caused minor part of the fast-flow stream's Y*l*m cycle (see in Example-12), Jupiter's major residue |5,4,4> QM state caused major part of the fast-flow zonal band's positive precession (see in Example-4), Jupiter's |5,4,4> QM state caused Jupiter's elliptical orbit (around the Sun, see in Table-3), the Sun (including Jupiter)'s residue nLL QM state caused its elliptical orbit around the Milky Way, the Sun (including Jupiter)'s residue nLL QM state caused its elliptical orbit's perihelion precession around the Milky Way, etc. Also, take example of Earth, not only the cycles of the continental drift, the polar jet, the elliptical orbit (around the Sun), but also the cycles of "El Nino vs. La Nina", Milankovitch cycles (see wiki "Milankovitch cycles"), etc., may also can be explained by the different levels of the residue nLL QM state caused positive precessions (or positive/negative precession cycles, or Y*l*m cycles).

V. Hypothesis: the residue nLL QM state's positive/negative precession may even be the origin of all the elliptic/parabolic/hyperbolic orbits (including the gravitational lensing)

When a planet is doing elliptic orbit motion around Sun (see in Figure 6, and also in Figure 7's green-line trajectory, in xy-2D plane), from the aphelion to perihelion to aphelion, it can be described as that it (the residue nLL QM state) is doing the positive/negative precession cycle (that equivalent to the Y*l*m cycle) with the n quantum number from high to low, then from low to high again.

When a propagating photon by-passing the Sun (or a black body), its original strait line trajectory is distorted by the Sun (through the general relativity effect) to become a parabolic/hyperbolic trajectory (illustrated in Figure 7 as the blue line trajectory in xy-2D plane). This parabolic/hyperbolic trajectory may can be described as that it (the residue nLL QM state) is doing the positive/negative precession cycle (that equivalent to the Y*l*m cycle) with the n quantum number from high to low, then to high again.

When a free-flying electron is scattered by a negatively changed atom, its original strait line trajectory is distorted to become a hyperbolic line trajectory (illustrated in Figure 7 as the red line trajectory in xy-2D plane). This hyperbolic

trajectory may can be described as that it (the residue nLL QM state) is doing the positive/negative precession cycle (that equivalent to the Y*l*m cycle) with the n quantum number from high to low, then to high again.

This discussion suggested that in a 2-body (or binary) interaction, the resulted elliptic/parabolic/hyperbolic trajectory (including the gravitational lensing) may can be explained by the residue nLL QM state's positive/negative precession cycle. In other words, in {N,n}QM field theory, the residue nLL QM state caused positive precession (or the positive/negative precession cycle) may be the origin of elliptic/parabolic/hyperbolic orbital motion (including the gravitational lensing).

Similarly, when an electron from far away is approaching a proton, its n changes from high to low to n=1, then the electron is trapped by the proton to form a H-atom. Also, when a photon from far away is approaching a black hole (BH), its n also changes from high to low to n=1, then the photon is trapped by the BH at the BH surface. Now I believed that this process may can be explained by the residue nLL QM state's positive precession. Furthermore, all (single) fusion process may can be explained by the (major) residue nLL QM state's positive precession. And, all (single) fission process may can be explained by the (major) residue nLL QM state's negative precession.

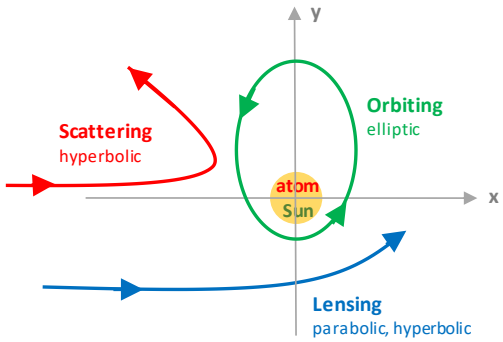

Figure 7. Illustration of an elliptic, a parabolic, or a hyperbolic orbital trajectory in a binary interaction.

VI. {N,n} QM, QCD, String Theory, GR, may all be the different "faces" of the same "Master Mechanics"

In text books, general relativity (GR) explains the lightspeed and its constancy, Mercury's perihelion precession, the special relativity's length contraction and the time dilation, the general relativity's radial contraction, the gravitational lensing, etc. Now in the {N,n} QM field theory, the quantum mechanics (QM) may can explain all of these (but in a very different way). Then, a big question is, is GR only a special situation of QM? Or, is the GR a parallel theory with QM at the same level, but currently only at an incomplete stage (just like QM was an incomplete theory before I discovered {N,n} QM)? I hope the answer is the later one. If so, then we really need someone to discover the rest part of GR, to make it become a complete theory.

Here is an alternative way to address the same point: the {N,n} QM research made me to believe that, the GR, the QCD, the string theory, the {N,n} QM, …, they are the different "faces" of the same "Master Mechanics". However, probably there is no single way to present this "Master Mechanics". You can only present the "Master Mechanics" by presenting all "faces" of this "Master Mechanics". (Note: See the similar description of the "Feynman Pool" in SunQM-6s8's Appendix-H). Furthermore, most of these theories are the half-completed theory right now, and need to be completed in the future.

Finally, because of its completeness and self-consistence, I do believe that the {N,n} QM is qualified to be put into the "Feynman Pool" as one of the many co-existing QM theories.

Conclusion

The pure QM may (intrinsically) generate a positive precession in a circular/elliptical orbital motion (or a binary motion), and this (intrinsic) positive precession may can be further developed to be a positive/negative precession cycle (i.e., the Y*l*m cycle).

Acknowledgements (of all SunQM series articles):

Many thanks to: all the (related) experimental scientists who produced the (related) experimental data, all the (related) theoretical scientists who generated all kinds of theories (that become the foundation of {N,n//q} QM theory), the (related) text book authors who wrote down all results into a systematic knowledge, the (related) popular science writers who simplified the complicated modern physics results into a easily understandable text, the (related) Wikipedia writers who presented the knowledge in a easily searchable/accessible way, the (related) online (video/animated) course writers/programmers who presented the abstract knowledge in an intuitive and visually understandable way. Also thanks to NASA and ESA for opening (and organizing) some basic scientific data to the public, so that citizen scientists (like me) can use it. Also thanks to the online preprinting serve vixra.org to let me to post out my original SunQM series research articles. Also thanks to the richness of the California state, and thanks to the high level of scientific research and the high level of the popular science education in USA, so that any civilized person in the world (with the good will) can use his own money (practically zero money) to do some studies on the theoretical physics (and using some free public resources).

Special thanks to: Fudan university, theoretical physics (class of 1978, and all teachers), it had made my quantum mechanics study (at the undergraduate level) become possible. Also thanks to Chen-Ning Yang and Tsung-Dao Lee, they made me to dream to be a theoretical physicist when I was eighteen. Also thanks to Shoucheng Zhang (张首晟, Physics Prof. at Stanford Univ., my classmate at Fudan Univ. in 1978) who had helped me to introduce the {N,n} QM theory to the scientific community in 2018.

Also thanks to a group of citizen scientists for the interesting, encouraging, inspiring, useful, and sometimes even amusing (online) discussions: "职老" (https://bbs.creaders.net/rainbow/bbsviewer.php?trd_id=1079728), "mingcheng99" (https://bbs.creaders.net/tea/bbsviewer.php?trd_id=1384562), "zhf" (https://bbs.creaders.net/tea/bbsviewer.php?trd_id=1319754), Yingtao Yang (https://bbs.creaders.net/education/bbsviewer.php?trd_id=1135143), "tda" (https://bbs.creaders.net/education/bbsviewer.php?trd_id=1157045), etc.

Also thanks to: Takahisa Okino (Correlation between Diffusion Equation and Schrödinger Equation. Journal of Modern Physics, 2013, 4, 612-615), Phil Scherrer (Prof. in Stanford University, who explained WSO data to me (in email, see SunQM-3s9)), Jing Chen (https://www.researchgate.net/publication/332351262_A_generalization_of_quantum_theory), etc. Note: if I missed anyone in the current acknowledgements, I will try to add them in the SunQM-9s1's acknowledgements.

Reference:

[1] Yi Cao, SunQM-1: Quantum mechanics of the Solar system in a {N,n//6} QM structure. http://vixra.org/pdf/1805.0102v2.pdf （original submitted on 2018-05-03）

[2] Yi Cao, SunQM-1s1: The dynamics of the quantum collapse (and quantum expansion) of Solar QM {N,n} structure. http://vixra.org/pdf/1805.0117v1.pdf （submitted on 2018-05-04）

[3] Yi Cao, SunQM-1s2: Comparing to other star-planet systems, our Solar system has a nearly perfect {N,n//6} QM structure. http://vixra.org/pdf/1805.0118v1.pdf （submitted on 2018-05-04）

[4] Yi Cao, SunQM-1s3: Applying {N,n} QM structure analysis to planets using exterior and interior {N,n} QM. http://vixra.org/pdf/1805.0123v1.pdf （submitted on 2018-05-06）

[5] Yi Cao, SunQM-2: Expanding QM from micro-world to macro-world: general Planck constant, H-C unit, H-quasi-constant, and the meaning of QM. http://vixra.org/pdf/1805.0141v1.pdf （submitted on 2018-05-07）

[6] Yi Cao, SunQM-3: Solving Schrodinger equation for Solar quantum mechanics {N,n} structure. http://vixra.org/pdf/1805.0160v1.pdf （submitted on 2018-05-06）

[7] Yi Cao, SunQM-3s1: Using 1st order spin-perturbation to solve Schrodinger equation for nLL effect and pre-Sun ball's disk-lyzation. http://vixra.org/pdf/1805.0078v1.pdf （submitted on 2018-05-02）

[8] Yi Cao, SunQM-3s2: Using {N,n} QM model to calculate out the snapshot pictures of a gradually disk-lyzing pre-Sun ball. http://vixra.org/pdf/1804.0491v1.pdf （submitted on 2018-04-30）

[9] Yi Cao, SunQM-3s3: Using QM calculation to explain the atmosphere band pattern on Jupiter (and Earth, Saturn, Sun)'s surface. http://vixra.org/pdf/1805.0040v1.pdf （submitted on 2018-05-01）
[10] Yi Cao, SunQM-3s6: Predict mass density r-distribution for Earth and other rocky planets based on {N,n} QM probability distribution. http://vixra.org/pdf/1808.0639v1.pdf (submitted on 2018-08-29)
[11] Yi Cao, SunQM-3s7: Predict mass density r-distribution for gas/ice planets, and the superposition of {N,n//q} or |qnlm> QM states for planet/star. http://vixra.org/pdf/1812.0302v2.pdf (replaced on 2019-03-08)
[12] Yi Cao, SunQM-3s8: Using {N,n} QM to study Sun's internal structure, convective zone formation, planetary differentiation and temperature r-distribution. http://vixra.org/pdf/1808.0637v1.pdf (submitted on 2018-08-29)
[13] Yi Cao, SunQM-3s9: Using {N,n} QM to explain the sunspot drift, the continental drift, and Sun's and Earth's magnetic dynamo. http://vixra.org/pdf/1812.0318v2.pdf (replaced on 2019-01-10)
[14] Yi Cao, SunQM-3s4: Using {N,n} QM structure and multiplier n' to analyze Saturn's (and other planets') ring structure. http://vixra.org/pdf/1903.0211v1.pdf (submitted on 2019-03-11)
[15] Yi Cao, SunQM-3s10: Using {N,n} QM's Eigen n to constitute Asteroid/Kuiper belts, and Solar {N=1..4,n} region's mass density r-distribution and evolution. http://vixra.org/pdf/1909.0267v1.pdf (submitted on 2019-09-12)
[16] Yi Cao, SunQM-3s11: Using {N,n} QM's probability density 3D map to build a complete Solar system with time-dependent orbital movement. https://vixra.org/pdf/1912.0212v1.pdf (original submitted on 2019-12-11)
[17] Yi Cao, SunQM-4: Using full-QM deduction and {N,n} QM's non-Born probability density 3D map to build a complete Solar system with orbital movement. https://vixra.org/pdf/2003.0556v2.pdf (replaced on 2021-02-03)
[18] Yi Cao, SunQM-4s1: Is Born probability merely a special case of (the more generalized) non-Born probability (NBP)? https://vixra.org/pdf/2005.0093v1.pdf (submitted on 2020-05-07)
[19] Yi Cao, SunQM-4s2: Using {N,n} QM and non-Born probability to analyze Earth atmosphere's global pattern and the local weather. https://vixra.org/pdf/2007.0007v1.pdf (submitted on 2020-07-01)
[20] Yi Cao, SunQM-5: Using the Interior {N,n//6} QM to Describe an Atom's Nucleus-Electron System, and to Scan from Sub-quark to Universe (Drafted in April 2018). https://vixra.org/pdf/2107.0048v1.pdf （submitted on 2021-07-06)
[21] Yi Cao, SunQM-5s1: White Dwarf, Neutron Star, and Black Hole Explained by Using {N,n//6} QM (Drafted in April 2018). https://vixra.org/pdf/2107.0084v1.pdf （submitted on 2021-07-13)
[22] Yi Cao, SunQM-5s2: Using {N,n//6} QM to Explore Elementary Particles and the Possible Sub-quark Particles. https://vixra.org/pdf/2107.0104v1.pdf (submitted on 2021-07-18)
[23] Yi Cao, SunQM-6: Magnetic force is the rotation-diffusion (RF) force of the electric force, Weak force is the RF-force of the Strong force, Dark Matter may be the RF-force of the gravity force, according to a newly designed {N,n} QM field theory. https://vixra.org/pdf/2010.0167v1.pdf (replaced on 2020-12-17, submitted on 2020-10-21)
[24] Yi Cao, SunQM-6s1: Using Bohr atom, {N,n} QM field theory, and non-Born probability to describe a photon's emission and propagation. https://vixra.org/pdf/2102.0060v1.pdf (submitted on 2021-02-11)
[25] Yi Cao, SunQM-7: Using {N,n} QM, Non-Born-Probability (NBP), and Simultaneous-Multi-Eigen-Description (SMED) to describe our universe. https://vixra.org/pdf/2111.0086v1.pdf (submitted on 2021-11-17)
[26] Yi Cao, SunQM-6s2: A Unified Description Of 1D-Wave, 1D-Wave Packet, 3D-Wave, 3D-Wave Packet, and |nlm> Elliptical Orbit For A Photon's Emission and Propagation Using {N,n} QM. https://vixra.org/pdf/2208.0039v1.pdf (submitted on 2022-08-08)
[27] Yi Cao, SunQM-6s3: Using {N,n} QM and "|nL0> Elliptical/Parabolic/Hyperbolic Orbital Transition Model" to Describe All General "Decay" Processes (Including the Emission of a Photon, a G-photon, or An Alpha-particle). (submitted on 2022-08-31, but has not been able to get posted out, I asked many times, no reply)
[28] Yi Cao, SunQM-6s4: In {N,n} QM Field Theory, A Point Charge's Electric Field Can Be Represented by Either the Schrodinger Equation/Solution, Or A 3D Spherical Wave Packet, In Form of Born Probability. https://vixra.org/pdf/2306.0136v1.pdf (submitted on 2023-06-23)
[29] Yi Cao, SunQM-6s5: Using {N,n} QM Field Theory to Describe A Propagating Photon as A 3D Spherical Wave Packet with the Oscillation Among Three QM States. https://vixra.org/pdf/2307.0098v1.pdf (submitted on 2023-07-18)
[30] Yi Cao, SunQM-6s6: Using {N,n} QM Field Theory to Study the Atomic Electron Configuration, the Pre-Sun Ball's {N,n} QM Structural Configuration, and the Nuclear Proton Configuration. https://vixra.org/pdf/2308.0118v1.pdf (submitted on 2023-08-18)
[31] Yi Cao, SunQM-6s7: The Face-to-face Tidal-locked Binary Orbital Rotation May Be the Origin of the Electron Spin and the Nucleon Spin. https://vixra.org/pdf/2310.0119v1.pdf (submitted on 2023-10-25)
[32] Yi Cao, SunQM-6s8: {N,n} QM Field Theory Development on the E/RFe-force, the G/RFg-force, and the Spin-spin Interaction. https://vixra.org/pdf/2311.0147v1.pdf (submitted on 2023-11-29)
[33] Yi Cao, SunQM-6s9: Reformulating Schrodinger Equation/Solution to Show Its r-1D Reversed-Diffusion Character for Solar System's {N,n} QM Structure Formation (Drafted in January 2020). https://vixra.org/pdf/2312.0101v1.pdf (submitted on 2023-12-19)
[34] Yi Cao, SunQM-6s10: {N,n} QM Field Theory, S/RFs-force, Nuclear Force, Spin-spin Interaction, and the Possible Origin of the Weak-Force and Beta-Decay. https://vixra.org/pdf/2406.0140v1.pdf (submitted on 2024-06-24)
[35] Yi Cao, SunQM-7s1: Space Formation/Transformation, Relativity, and the Possible Origin of the Lightspeed and Its Constancy (Viewed From the {N,n} QM). https://vixra.org/pdf/2407.0170v1.pdf (submitted on 2024-07-29)
[36] Yi Cao, SunQM-7s2: The Possible Origins of the Relativistic Length Contraction, E=mc^2, and to Fuse the General Relativity's Radial Contraction with the Non-Linear {N,n} QM. https://vixra.org/pdf/2408.0050v1.pdf (submitted on 2024-08-12).
[37] Neil F. Comins & William J. Kaufmann, "Discovering the Universe", pp328, Figure 10-13, Babcock's magnetic dynamo.
[38] Neil F. Comins & William J. Kaufmann, "Discovering the Universe", pp327, Figure 10-12b.

[39] Copied from "https://phys.libretexts.org/Bookshelves/Astronomy__Cosmology/Astronomy_1e_(OpenStax)/11%3A_The_Giant_Planets/11.03%3A_Atmosphere_of_the_Giant_Planets". Authored, remixed, and/or curated by OpenStax. Copyright: CC BY 4.0.
[40] 周世勋, 量子力学教程, (Shi-Xun Zhou, Quantum Mechanics Tutorial) 1979 edition, p62, eq-3.2-18.
[41] Douglas C. Giancoli, Physics for Scientists & Engineers with Modern Physics, 4th ed. 2009, p1046.
[42] David J. Griffiths, Introduction to Quantum Mechanics, 2nd ed., 2017, p152, eq-4.84.

Note: A series of SunQM papers that I am working on:
SunQM-8: {N,n} QM and the condensed matter physics … (drafted in Jan. 2024).
SunQM-9s1: Addendums, Updates and Q/A for SunQM series papers. (in drafting since 2019).

Note: Major QM books, data sources, software that I used for the study (in the SunQM series papers):
Douglas C. Giancoli, Physics for Scientists & Engineers with Modern Physics, 4th ed. 2009.
David J. Griffiths, Introduction to Quantum Mechanics, 2nd ed., 2015.
Stephen T. Thornton & Andrew Rex, Modern Physics for Scientists and Engineers, 3rd ed. 2006.
John S. Townsend, A Modern Approach to Quantum Mechanics, 2nd ed., 2012. (Figure 9.11, Figure 10.5)
周世勋, 量子力学教程, (Shi-Xun Zhou, Quantum Mechanics Tutorial) 1979 edition.
Wikipedia at: https://en.wikipedia.org/wiki/
(Free) online math calculation software: WolframAlpha (https://www.wolframalpha.com/)
(Free) online spherical 3D plot software: MathStudio (http://mathstud.io/)
(Free) offline math calculation software: R
Microsoft Excel, Power Point, Word.
Public TV's space science related programs: PBS-NOVA, BBC-documentary, National Geographic-documentary, etc.
Journal: Scientific American.

Note: I am still looking for endorsers to post all my SunQM papers (including the future papers) to arXiv.org. Thank you in advance!
So far, my identity (for the {N,n} QM development) is: a former lecturer of Fudan University, and a (10 years closed-door, 2014 ~ 2024) citizen scientist of California.

Note: With my 37 of SunQM papers that have been posted out so far, I believe that the framework of the {N,n} QM has been fully established. It is clear now that the {N,n} QM description is suitable not only for the mass field, but also for the force field (or the energy field, etc.). Thus, my (10 years of closed-door) research phase on the {N,n} QM will end (most likely in the summer of 2024). After that, I will re-write the SunQM papers (~ 37 of them) in form of a text book. The initial plan is, 1) Try to formally publish all ~37 of SunQM papers as the original version (version-1, or version 2018) if possible; 2) Using ~2 years, to brief (by re-writing) all ~37 of SunQM papers (as version-2, or version 2025), the main purpose is to unify the nomenclature and the description, compress the total words from over 400,000 to less than 200,000, (and publish it if possible), make it ready for the text book writing; 3) Using 2 ~ 4 years, to write a Bohr-QM based {N,n} QM text book with ~ 100,000 words (as version-3, for college and high-school students), formally publish it if possible, and may make a few online video lectures; 4) Using 2 ~ 4 years, to add Schrodinger-equation based {N,n} QM into the version-3 text book with final ~ 200,000 words (as version-4), formally publish it if possible, and may make a few online video lectures. It may take me total 6 ~10 years (2024 ~ 2035, semi-retired) to finish all the work. I may go back to Shanghai to do this work, either as a citizen scientist of Shanghai, or, if lucky, as a (semi-retired) professor in Fudan university.

Appendix A. A more complicated explanation for SunQM-6s11's Fig-5. (A note only for myself).

Alternatively, a more complicated (and hopefully more accurate) explanation for Figure 5 is: the "φ-1D bi-direction motion" (of the two virtual angular momentum vectors ($\vec{\boldsymbol{L}}_{\pm\boldsymbol{z}}$) in φ-1D) is transformed into (or equivalent to) two virtual angular momentum vectors $\vec{\boldsymbol{L}}_{\pm\boldsymbol{\theta}}$ that are doing the "θ-1D bi-directional motion" (as shown in Figure 8). Then, according to Figure 5a, Figure 8 can also be (more precisely) explained as: while the vector $\vec{\boldsymbol{L}}_{\pm\boldsymbol{\theta}}$ is turning around in both ±θ bi-directions in the $\vec{\boldsymbol{L}}_{\boldsymbol{\theta}}$-1D space, the $\vec{\boldsymbol{L}}_{\boldsymbol{x}}$-1D is also turning around in both ±φ bi-directions in the $\vec{\boldsymbol{L}}_{\boldsymbol{\varphi}}$-1D space. Therefore, for a ~100% mass-occupied spherical body, in the nLL QM state (i.e., in the equatorial region), its $\vec{\boldsymbol{L}}_{\pm\boldsymbol{z}} \rightarrow \vec{\boldsymbol{L}}_{\pm\boldsymbol{\theta}}$ QM effect will cause a ±|m| cycle, with half period in +|m| state, and half period in -|m| state. There may have three different cases for the ±|m| cycle:

"±m cycle" case-1: if both transformed virtual $\vec{\boldsymbol{L}}_{\pm\boldsymbol{z}} \rightarrow \vec{\boldsymbol{L}}_{\pm\boldsymbol{\theta}}$ vectors start their ±m cycle (or the "θ-1D bi-directional motion") at θ = 0 (that is, the 1st one starts at θ = 0, the 2nd one starts with a phase difference Δθ = 0 to the 1st one), it will have the maximum add-up of the ±m value, therefore, it will produce the strongest ±m cycle effect (as shown in Figure 5b).

(Note: in this case, both the original virtual $\vec{L}_{\pm z}$ vectors (that before the transforming) may should also be both at φ = 0 position to start the "φ-1D bi-direction motion"). (Note: May this match to that in the macro-world, a single mass entity must be at a single position in φ-1D, although its QM shows that it has ±φ bi-direction motion simultaneously?).

"±m cycle" case-2: if the transformed virtual $\vec{L}_{\pm z} \rightarrow \vec{L}_{\pm \theta}$ vectors start their ±m cycle with one at θ = 0 and another one at θ = π (that is, the 1st one starts at θ = 0, the 2nd one starts with a phase difference Δθ = π to the 1st one), it will fully cancel off the ±m value, therefore, it will produce the zero ±m cycle effect. (Note: In this case, for the two original virtual $\vec{L}_{\pm z}$ vectors that are doing the "φ-1D bi-direction motion" before transforming, one may start at φ = 0 position and the second one may start at φ = π position). (Question: in this case, only positive precession?).

"±m cycle" case-3: if the both transformed virtual $\vec{L}_{\pm z} \rightarrow \vec{L}_{\pm \theta}$ vectors start their ±m cycle at 0 < θ < π (that is, the 1st one starts at θ = 0, the 2nd one starts with a phase difference 0 < Δθ < π to the 1st one), it will partly cancel off the ±m value. Therefore, it will produce a weaker ±m cycle effect than that in the case-1.

Note: if this discussion is correct, then all examples in the section III are assumed that they are in **"±m cycle" case-1** with the maximum ±m cycle effect.

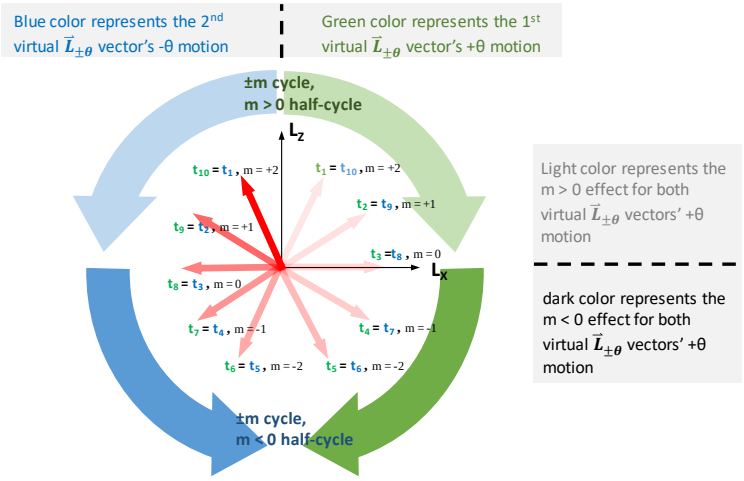

Figure 8. Illustration that the two virtual angular momentum vectors ($\vec{L}_{\pm z}$) in φ-1D bi-direction is transformed into two virtual angular momentum vectors $\vec{L}_{\pm \theta}$ that are doing the "θ-1D bi-directional motion", and in "±m cycle" case-1.

Appendix B. Does the Y*l*m cycle progresses always from low n to higher n'? (A note only for myself).

1) For the sunspot drift, during the positive precession half-cycle, the Y*l*m cycle progresses from low n to higher n', the stream speed changes from fast to slow (to match the background). However, during the negative precession half-cycle, does the Y*l*m cycle progresses also from low n to higher n', but the stream speed changes from slow to fast (to match the background)?

2) In SunQM-6s8's section III-b-6, I said: "*we see that for the same pre-Sun ball, a disk-lyzation (i.e., disk-forming) process is a nLL effect evolution process that from the low n (or the basic n) to high n', and this is very similar as the Ylm cycle process that also from the low n (or the basic n) to high n', or a photon propagation process that also from the low n (or the basic n) to high n'* ".

2a) In the θ-1D, during the disk-forming process of the pre-Sun ball, Δθ' changed from large to small, actually it is the nLL QM state's n number increase from low to high. For example, Earth from n = 5 of the |5,4,4> QM state to n = 5*6^1 of |30,29,29> , then to n = 5*6^2 of |180,179,179> , etc.

2b) In the r-1D, during the ring-forming process after the pre-Sun ball's disk had formed, Δr from large to small, actually it is also the nLL QM state's n number increase from low to high. For example, Earth from n = 5 of the |5,4,4> QM state to n = 5*6^1 of |30,29,29> , then to n = 5*6^2 of |180,179,179> , etc.
2c) In the φ-1D, during the accretion process, from Δφ decreased from 2π to ~ 0, it is also the n increase from low to high.

3) The ABCBA cycle that used to describe the photon propagation process (in SunQM-4s4) may be also one kind of Y*l*m cycle.

4) For ~100% mass occupancy, the major residue nLL QM state causes the fast-flow stream, and the minor residue nLL QM state causes the Y*l*m cycle. For < 1% mass occupancy, does the major residue nLL QM state causes an elliptic orbital motion (one kind of Y*l*m cycle), and the minor residue nLL QM state causes the elliptic orbital perihelion positive precession (during the Y*l*m cycle)?

5) At low n, position distribution may be more uncertain, and may be more effective wave description. At higher n', position distribution may be more certain, and may be more effective particle description. Similar as that in the classical physics, all objects have "accurate" position, so they will have high n number in QM.

Appendix C. Does the progressing of Y*l*m cycle is from low n to high n', and it causes the minor residue nLL QM state fast-flow stream (in the positive precession half-cycle) to become shallower, narrower, slower, and finally to disappear in the background? And also, does it also caused the minor residue nLL QM state slow-flow stream (in the negative precession half-cycle) to become shallower, narrower, faster, and finally to disappear in the background? (A note only for myself).

This is the explanation that I was pursuing for the Y*l*m cycle, but is not successful yet. Let me using the progressing of the sunspot drift on the Sun surface as the example to explain. (Notice that Sun follows {N,n//6} QM structure).

First, according to SunQM-6s10's eq-8, $|\Theta(\theta)|^2 \propto [\sin(\theta)]^{2(n-1)}$, the θ-1D distribution of Born probability of |2,1,1> QM state at $|Y_{\theta,\varphi}(1,1)|^2 = |\Theta(\theta)|^2\,|\Phi(\varphi)|^2$, (see eq-3), was plotted in Figure 9a, with either the base n = 2, or the high-frequency n'= 2*6^1 = 12, or n' = 2*6^3 = 432. We can see that in Figure 9a, from |2,1,1> to |12,11,11> to |432,431,431>, as the n' number increases (or as the r_1 is moved inward), the residue nLL QM state stream become narrower, from Δθ' around ±30°, to around ±11°, and to around ±2° latitude range. Then, from Figure 10a, we see that the progress of the observed sunspot is from around ±30° latitude gradually down to the equator. It well matches the hypothesis that the sunspot may start at the residue |2,1,1> QM state, and then progress to higher n' numbered residue nLL QM state, and finally disappeared at (assumed) n' → ∞.

Second, according to SunQM-6s10's eq-5, $r^2|R(n,l=n-1)|^2 \propto \left(\frac{r}{r_n}e^{1-\frac{r}{r_n}}\right)^{2n}$, the r-1D distribution of Born probability of |2,1,1> QM state (with $r_1 = 1$ and $r_{n=2} = 4$, or maximum at $r/r_1 = 4$) was plotted in Figure 9b, at either the base n = 2, or the high-frequencies n' = 2*6^1 = 12 and n' = 2*6^3 = 432. We can see that as the residue |2,1,1> QM state progressed to higher n' number |12,11,11>, or |432,431,431>, the correlated minor residue nLL stream gets shallower (to the surface of the Sun equator at $r/r_1 = 4$, because Sun as a size of {0,2//6}).

Third, according to Table 4, we see that as the residue |2,1,1> QM state progressed to higher n' number |12,11,11>, or |432,431,431>, the residue nLL QM state stream gets slower and slower. (Note: This is certainly suitable for $0.5\pi < x \leq \pi$ in Figure 10b, although whether it is suitable for $0 < x \leq 0.5\pi$ in Figure 10b is still unclear).

Therefore, the above three calculations supported the explanations that as the sunspot drifting from high latitude to zero latitude, the minor residue |2,1,1> stream is getting narrower, shallower, and slower (at least for $0.5\pi < x \leq \pi$ in Figure 10b).

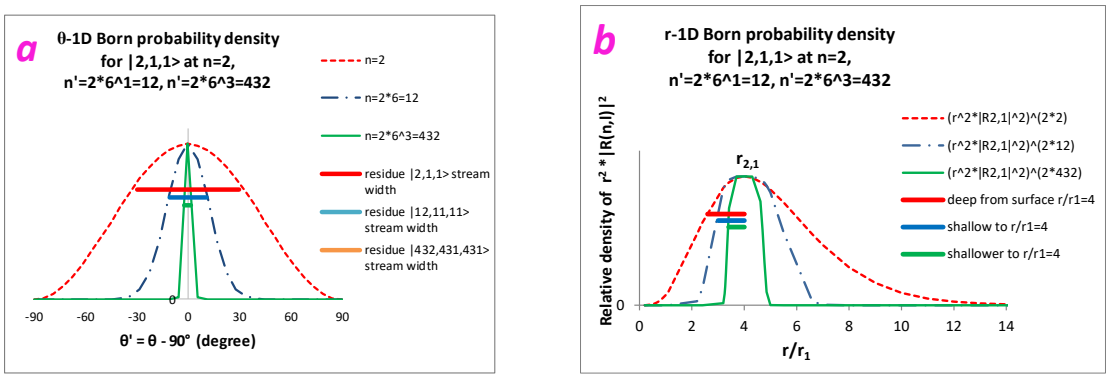

Figure 9a. Born probability distribution in θ-1D at nLL QM state of |2,1,1>, |12,11,11>, and |432,431,431>.
Figure 9b. Born probability distribution in r-1D at nLL QM state of |2,1,1>, |12,11,11>, and |432,431,431>.

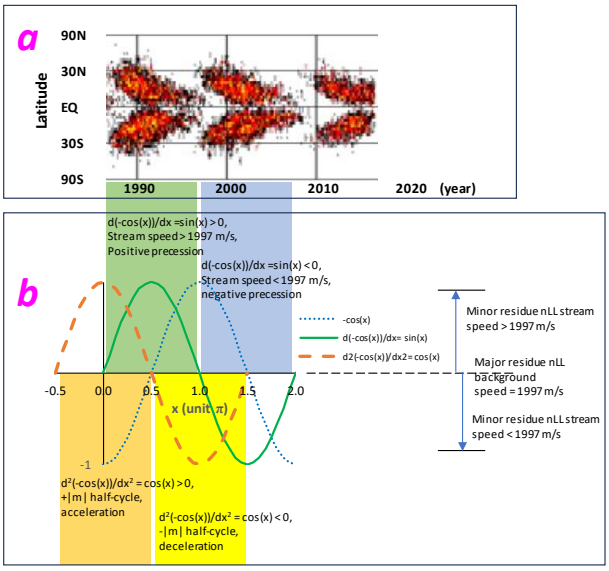

Figure 10a. The Butterfly diagram of the sunspots. Copied from wiki "Sunspot". Author: NASA. Copyright: Public Domain.
Figure 10b. A designed Y*l*m cycle that is used to explain the sunspot drift cycle with 22 years period. Note: The alignment between Figure 10a and Figure 10b may or may not have ½ cycle (11 years) phase shift.

Based on the above new knowledge, by referencing the Newtonian mechanics (i.e., distance x, velocity $\frac{dx}{dt}$, acceleration $a = \frac{d^2x}{dt^2}$, and the force F = ma), and by using the trigonometry (i.e., $\frac{d(\sin(x))}{dx} = \cos(x)$ and $\frac{d(\cos(x))}{dx} = -\sin(x)$), I tried to design a new explanation for the sunspot drift as shown in Figure 10, and it is explained below.

Design-1. In Figure 10a, in the sunspot's 22 years (1986 ~ 2008) cycle, suppose the 1986~1997 half-cycle is caused by the minor residue |2,1,1> fast-flow steam, and the 1997~2008 half-cycle is caused by the minor residue |2,1,1> slow-flow steam. See in Figure 10b's green solid-line curve, I used a $\sin(x) = \frac{d(-\cos(x))}{dx}$ wave function to represent the relative speed of the minor residue |2,1,1> stream (that relative to the speed of the neighboring background 1997 m/s in the major residue |2,1,1> fast-flow stream), with the positive amplitude half period of $0 < x \leq \pi$ represents the speed faster than 1997 m/s, and the negative amplitude half period of $\pi < x \leq 2\pi$ represents the speed slower than 1997 m/s. Notice that at $x = 0.5\pi$ and 1.5π, the

positive/negative peak of sin(x) represents the maximum speed difference between the minor residue nLL stream to the background 1997 m/s, and thus produces the maximum number of sunspots in year 1991 and 2002.

Design-2. See in Figure 10b's orange dashed-line curve, I used a $\cos(x) = \frac{d(\sin(x))}{dx} = \frac{d^2(-\cos(x))}{dx^2}$ wave function to represent the acceleration/deceleration for the speed of the minor residue |2,1,1> stream. It maybe correlate to apply a force to accelerate a mass body in the Newtonian mechanics (i.e., F = ma = $m\frac{d^2x}{dt^2}$). Notice that the whole acceleration phase ($-0.5\pi < x \leq 0.5\pi$) is ¼ cycle-period ahead of the faster than 1997 m/s phase ($0 < x \leq \pi$), and the whole deceleration phase ($0.5\pi < x \leq 1.5\pi$) is ¼ cycle-period ahead of the slower than 1997 m/s phase ($\pi < x \leq 2\pi$). (Note: This ¼ cycle-period ahead is also true for the elliptic orbit motion shown in Figure 6).

Design-3. See in Figure 10b's blue dotted-line, I used a -cox(x) wave function to represent the (relative) distance that the minor residue |2,1,1> stream flowed relative to the background flow. When x from 0π to 0.5π to π, the minor residue |2,1,1> stream flowed-distance is from behind the background flowed-distance, to catch up the background flowed-distance, and then to ahead the background flowed-distance, respectively. In Figure 10b, the relative flowed-distance change is ¼ cycle-period behind of the speed change, and 2/4 cycle-period behind of the acceleration change. Thus, design-1, design-2, and disign-3, (i.e., -cos(x) for the relative distance, $\frac{d(-\cos(x))}{dx} = \sin(x)$ for speed change, and $\frac{d^2(-\cos(x))}{dx^2} = \cos(x)$ for the acceleration change), fully matches the Newtonian mechanics (i.e., x for distance, $\frac{dx}{dt}$ for speed, $\frac{d^2x}{dt^2}$ for acceleration).

Design-4. Finally, I attributed that the driving force to accelerate/decelerate the minor residue nLL stream comes from the pure quantum mechanics, i.e., the +/- m cycle caused positive/negative precession cycle (that is equivalent to the Y*l*m cycle). I guessed that the +|m| half-cycle (in Figure 8) is the driving force to accelerate the minor residue nLL stream speed (shown in Figure 10b as $\frac{d^2(-\cos(x))}{dx^2} = \cos(x)$ in range of $-0.5\pi < x \leq 0.5\pi$), and the -|m| half-cycle (in Figure 8) is the driving force to decelerate the minor residue nLL stream speed (shown in Figure 10b as $\frac{d^2(-\cos(x))}{dx^2} = \cos(x)$ in range of $0.5\pi < x \leq 1.5\pi$).

Problem of the design: Design-1 through Design-3 looks good. In the Design-4, the phase of +|m| and -|m| in Figure 8 is hard to match the phase of |m| = n' – 1 (for the nLL state) in Figure 10b. Also, it is hard to determine the n' curve. For example, is it a csc(x) = 1/sin(x) curve that with n' decreasing first, then increasing during $0 < x \leq \pi$ (note: this better matches the elliptic/parabolic/hyperbolic orbit in which n' decreases first and then increases)? Or, is n' always increasing during $0 < x \leq \pi$ (e.g., when x from 0π to 0.5π to π, n' from sub-base-n, to base-n =2, then to high-frequency n')? Or, in other kind of curve? However, this is the best I can do so far, and I may will re-design it in the future (just like before I had designed an older version of this explanation in SunQM-3s9's Fig-8).